Detection and quantification of lateral, illicit connections and infiltration in sewers with Infra-Red camera: conclusions after a wide range of experiments

Konstantinos Makris

TU Delft Delft University of Technology

Detection and quantification of lateral, illicit connections and infiltration in sewers with Infra-Red camera: conclusions after a wide range of experiments

by

Konstantinos Makris

in partial fulfilment of the requirements for the degree of

Master of Science

in Civil Engineering

at the Delft University of Technology,

to be defended publicly on Tuesday July 5, 2016 at 10:00 AM.

Thesis committee:

Prof.dr.ir. F. Clemens	Delft University of Technology Sanitary Engineering Section
Dr. M. Lepot	Delft University of Technology Sanitary Engineering Section
Ir. W.M.J. Luxemburg	Delft University of Technology Water Resources Section

TU Delft Delft University of Technology

Detection and quantification of lateral, illicit connections and infiltration in sewers with Infra-Red camera: conclusions after a wide range of experiments.

Konstantinos F. MAKRIS[1]

[1] Water Management Department, Faculty of Civil Engineering and Geosciences, Delft University of Technology, Stevinweg 1 (Building 23), 2628 CN Delft, The Netherlands

Abstract

The most known problem of separate sewer systems is the existence of illicit connections and, hence, the deposition of untreated sewage to the receiving waters or the occurrence of urban flooding due to overloading of wastewater systems with storm water. Although there are several known and relative expensive techniques for inspection of storm sewer systems (e.g. smoke or sound based technologies), most of them concentrate on the structural or operational reliability of the inspected pipe and ignore the conditions that prevail beneath the surface of the water, detecting only some defects. An infrared camera (Flir A35) was used for a more comprehensive approach towards the inspection of a storm sewer pipe, by identifying abnormal thermal finger prints (due to lateral connections) along a flume. The illicit connections were simulated by discharging warm or cold water through several types of lateral connections (variation of diameter, intrusion, depth, etc.). Data analysis revealed that the detection and quantification of illicit connections is possible, albeit under certain conditions.

Keywords: IR camera, on-line measurement, sensor, calibration method, accuracy, robustness, water quality.

List of Symbols

Symbols	Description	Dimension/ Unit
A_{TANK}	Area of the tank	L^2/m^2
B, R, O, F	Planck constants	-/-
d	Duration of the experiment	T/s
$D_{M,i,j}$	The jth measurement for the estimated distance i	L/m
$d_{M,i,j}$	The jth measurement for the distance i	L/m
$D_{R,i}$	Estimated by the calibration model distance of index i	L/m
$d_{R,i}$	Real distance of index i	L/m
$h_{BEGINNING}$	Water level in the tank at the beginning of the experiment	L/m
h_{END}	Water level in the tank at the end of the experiment	L/m
k1, k2, k3	Radial distortion coefficients of the lens	-/-
N_{CD}	Number of calibration distances	-/-
N_M	Number of measurements per calibration distance	-/-
p1, p2	Tangential distortion coefficients of the lens	-/-
Q_D	Discharge of the main pipe downstream	$L^3\ T^{-1}/m^3\ s^{-1}$
Q_{LC}	Discharge of the lateral connection	$L^3\ T^{-1}/m^3\ s^{-1}$
$Q_{LC,TRUE}$	Known discharge of the lateral connection	$L^3\ T^{-1}/m^3\ s^{-1}$
Q_U	Discharge of the main pipe upstream	$L^3\ T^{-1}/m^3\ s^{-1}$
T	Temperature	τ/°C
T_D	Temperature of the main pipe downstream	τ/°C
T_i	Pixel temperature at frame i	τ/°C
T_{LC}	Temperature of the lateral connection	τ/°C
$T_{LC,EST-COLD}$	Estimated temperature of the cold lateral connections	τ/°C

Symbols	Description	Dimension/ Unit
$T_{LC,EST-WARM}$	Estimated temperature of the warm lateral connections	τ/°C
T_U	Temperature of the main pipe upstream	τ/°C
x, y	Undistorted pixel coordinates	-/-
$x_{DISTORTED}$, $y_{DISTORTED}$	Distorted pixel coordinates	-/-
$\sigma(A_{TANK})$	Uncertainty of the area of the tank	L^2/m^2
$\sigma(d)$	Uncertainty of the duration of the experiment	T/s
$\sigma(d_{M,i})$	Standard deviation of $d_{M,i}$	L/m
$\sigma(d_{R,i})$	Standard deviation of $d_{R,i}$	L/m
$\sigma(h_{BEGINNING})$	Uncertainty of the water level in the tank at the beginning of the experiment	L/m
$\sigma(h_{END})$	Uncertainty of the water level in the tank at the end of the experiment	L/m
$\sigma(Q_{LC})$	Uncertainty of the discharge of the lateral connection	$L^3\ T^{-1}/m^3\ s^{-1}$
$\sigma(Q_{LC,TRUE})$	Uncertainty of the known discharge of the lateral connection	$L^3\ T^{-1}/m^3\ s^{-1}$
$\sigma(Q_U)$	Uncertainty of the discharge of the main pipe upstream	$L^3\ T^{-1}/m^3\ s^{-1}$
$\sigma(T_D)$	Uncertainty of the temperature of the main pipe downstream	τ/°C
$\sigma(T_i)$	Uncertainty of the pixel temperature at frame i	τ/°C
$\sigma(T_{LC})$	Uncertainty of the temperature of the lateral connection	τ/°C
$\sigma(T_U)$	Uncertainty of the temperature of the main pipe upstream	τ/°C

1. Introduction

Sewer systems are generally capital extensive and aging structures. Along their lifetime, *i.e.* from their construction to their replacement, they are liable to several defects (coded

in ENV 13508) and misconnection occurrences. Both aspects have been widely treated by research studies (e.g. Chandler and Lerner, 2015).

The most widely used technique for sewer inspection (CCTV: Closed Circuit Television cameras) is known to be rather inaccurate and subjective (Dirksen *et al.*, 2011). In order to withdraw those drawbacks, recent developments suggest new sewer inspection techniques, sometimes based on the laser profiling (Clemens *et al.*, 2014). This technique, although accurate (standard uncertainty of 1.1 - 1.8 mm, Stanic, 2016), lacks: *i)* a camera (in the visible range and under good light condition) to establish a qualitative diagnostic (Lepot *et al.*, 2016), and *ii)* capacities to be used without disruption of the sewage service.

The wastewater of approximately 25% of the households in the Netherlands is discharged into separate sewer systems (Schilperoort *et al.*, 2013). This tendency for using separate systems for the discharge of different types of water could be easily justified by the several advantages that separate systems are supposed to have (reduction of health risks, reduction of environmental effects and recycling of run-off water, *etc.*). However, the major disadvantage that is usually observed is the existence of illicit or mis-connections. The combination with the absence of inspection or treatment of storm water results in the direct discharge of raw sewage to the receiving waters.

Very commonly used techniques (Panasiuk *et al.*, 2015) for the detection of illicit connections are the smoke test and the dye test (Hoes *et al.*, 2009), and the use of fiber-optic distributed temperature sensing (DTS, Nienhuis *et al.*, 2013, Hoes *et al*, 2011). While, for most cases, the inspection is usually restricted by the water level within the pipe, the current research strives to give a more comprehensive approach to the detection of illicit connections and groundwater infiltration with the use of

thermography. Several purposes can be reached by the different kind of inspection techniques: *i)* the detection of potential misconnection(s), *ii)* their localisations and *iii)* their quantifications. Those techniques can offer data over the time, the space or both: the records of time series, as temperature (Schilperoort *et al.*, 2006) or conductivity (Deffontis *et al.*, 2013), allow the detection and, sometimes, the quantification (e.g. in de Bénédittis and Bertrand-Krajewski, 2005) of lateral connections or/and infiltrations. However, due to the single place location of the sensor, the localisation of the misconnection is not feasible. Other techniques provide a spatial detection: visual inspections (Butler and Davies, 2004), sometimes combined with the temporal sensitivity as for DTS (Hoes *et al.*, 2009). Most of the techniques reviewed by Panasiuk *et al.* (2015) present some drawbacks: DTS require the installation of the fibre in sewer, dye and smoke testing are time consuming, odour or visual inspection are, by definition, sensitive to human subjectivity and methods based on sample analysis may be costly.

In order to present a new inspection technique, not only limited to misconnection, but as well for other defects, the FOULC (Fast Overall scanning of Underground and Linear Construction) platform is under development. This is a hovercraft drone, which will consist of several sensor devices: laser profiler, sonar, velocity/turbidity profiler, cameras (IR, visible and UV range). Some of them have already been tested in other PhD or MSc thesis: a laser profiler (Ibak, ILP) and a velocity profiler (Ubertone, UB Flow). The main purpose is the creation of a new sewer inspection tool, which is able to provide a comprehensive view of the structural, operational and hydraulic conditions in sewer systems. On the ground of this research an Infrared Camera (Flir, A35sc) was used as Lega and Napoli (2010), but within the sewer, in order to allow a spatial detection of active (leaking) lateral connection: a lateral connection without any flow cannot be identified by the presented technique.

Based on a basic thermodynamic balance, a quantification method is proposed and tested on a large number of laboratory experiments. Detection and quantification capabilities of this technique are finally detailed and discussed.

2. Materials and methods

2.1. Experimental set up

Experiments have taken place on the Eastern Scheldt flume in Deltares. The experimental setup was divided in three parts.

The main flume. This rectangular channel is built with glass windows and a steel structure: 1 m width, 1.2 m high and 50 m long (42 m of glass windows + start and end in concrete, Fig. 1). Supplied by a pump (Floweserve, MI10), the flow is controlled by frequency of the supply and measured with an electromagnetic flowmeter (Endress+Hauser, Promag W) of 600 mm. Hydraulic conditions are controlled by a wall valve located downstream.

Figure 1. The experimental setup: Image of the right bank of the Eastern Scheldt flume.

The sensor train. On top of the steel structure, a railway allows the perfectly parallel translation of the moving structure. On this train, an uncooled IR camera (Flir, A35sc)

and an accurate distance meter (Dimetix, FLS-C10, for details see Stanic (2016)) have been installed and connected to their respective data acquisition systems (laptop computers). Figure 2 presents the two data acquisition systems. This platform was manually moved during the experiments and its position was recorded by the laser data.

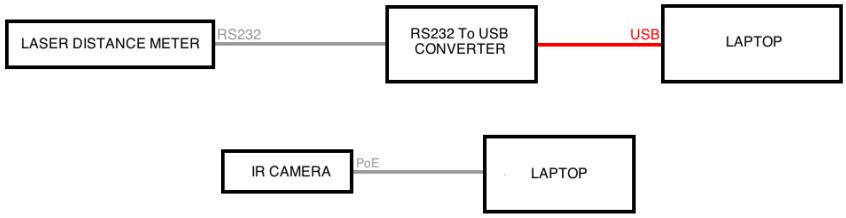

Figure 2. Schemas of the two data acquisition systems.

The synchronization between the two systems was achieved by placing relatively warm objects within the field of view of the IR camera, and removing them at the moment that the sensor train began to move. This procedure required some pre-processing action for every experiment, in order to track which frame corresponds to the first moving point of the structure, as it was recorded by the laser distance meter.

The tank and the lateral connections. In order to simulate lateral connections, special windows with several connection types (Table 1, Fig. 3 & 4) have been mounted on the flume. Lateral connections have been supplied with warm (heated with a pasteuriser - TomPress, Pasteurisateur thermoplongeur à jus) and cold (cooled with crushed ice) water, stored in a 0.91 m^3 tank.

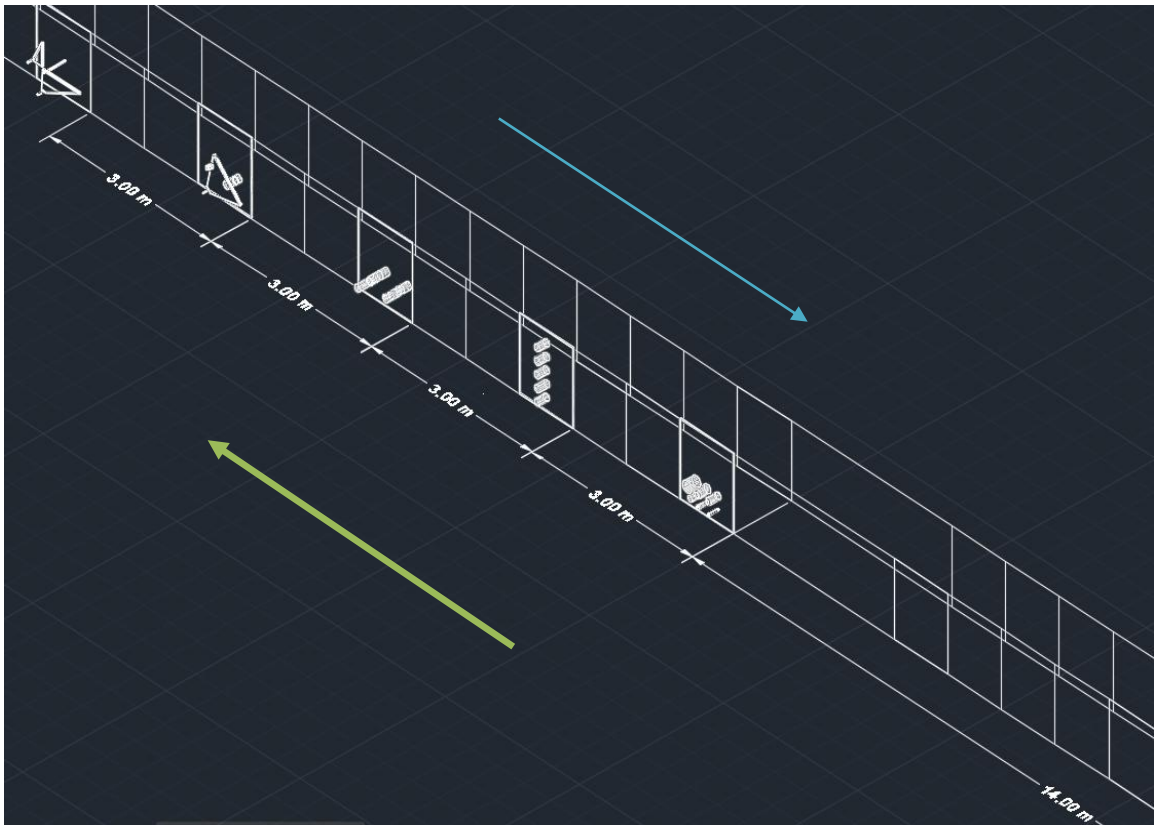

Figure 3. AutoCAD© sketch of the windows in the flume. The blue array indicates the motion of water. The green array indicates the movement of the sensor train.

Figure 4. The experimental setup: photo of the diameter windows set up on the right bank of the Eastern Scheldt flume.

Table 1. List of lateral connections (Sketchup© screenshots are presented in Appendix A).

Windows	Name of connection	Description
Diameters	D 200 mm D 160 mm D 100 mm	Several diameters, located at 400 mm from the invert level (center of the connection)
Water levels	WL 200 mm WL 400 mm WL 600 mm WL 800 mm WL 1 000 mm	100 mm diameter, located at several water level i.e. from invert level (center of the connection)
Intrusion	I 50 mm I 100 mm I 150 mm I 200 mm	100 mm diameter, located at 200 mm (I 100 and I 200) and 400 mm (I 50 and I 150) from the invert level (center of the connection)
Diffuser	Di 0 Di 45 Di 90	Line of 5mm diameter hole (1 every 10mm)
Mixed	Di - 45 D 75 mm I 50 mm	Mixed condition windows: I 50 is 100 mm diameter (center located at 400 mm from the invert level)

In order to ensure a uniform distribution of the temperature, water has been mixed with a mixer equipped with a pitched 3 blade propeller (Shaft length: 650mm, Shaft diameter: 30mm, Overall diameter: 170mm): rotation frequency has been fixed to 30 Hz. A 10 m pipe (50 mm of diameter) has been used for the connection between the tank and the special windows. In order to ensure connection with small diameters

(Table 1, diffuser and mixed – Di connection), an extra pipe (32 mm, 2 m) has been added (with a 50-32 mm diameter reduction) while needed. Discharges from the tank to the flume have been controlled with a manual quarter valve and calculated via lost volume (difference in water levels, before and after the opening, measured with a ruler) and the opening duration (recorded by a chronometer application).

2.2. Laboratory experiments

Hundreds (to be exact: 898) of experiments have been done within a period of two months. Each lateral connection (Table 1) has been tested with warm and cold water, for each hydraulic condition in the flume (Table 2) and for three valve openings (from the tank to the flume: 100, 50 and 10 %).

Table 2. List of the hydraulic conditions during the experiments.

Code for the experimental conditions	Discharge in the flume - upstream the lateral connection (Q_U) (m^3/s)	Position of the wall valve (m)	Average velocity at 20 m from the wall valve (m/s)	Reynolds number (without unit) $N_{RE} = u * d_h/v$
1a	0.1	0.70	0.12	150000
	0.1	0.30	0.23	210000
1b	0.12	0.30	0.26	250000
2	0.2	0.60	0.25	300000
3	0.3	0.50	0.38	465000
4	0.4	0.40	0.54	640000
5a	0.5	0.30	0.71	825000
5b	0.52	0.30	0.72	850000

Additionally to all the combinations, other experiments have been performed: blank measurements for each hydraulic condition, repeated measurements (by

triplicates), and measurements with different moving speed of the IR camera. In total, 898 experiments have been done.

2.3. Methods

2.3.1. Sensor calibration

Both uncooled IR camera and laser distance meter need to be calibrated.

IR camera calibration. IR cameras present vignetting and distortion phenomena due to optical effects in the lens applied. Despite the fact that calibration of standard camera is easy with a checkerboard (Bouguet, 2004), the calibration of IR camera presents some additional difficulties. The IR camera has just been calibrated for tangential and radial distortion (Eqs. 1), in three steps. Firstly, a black and white checkerboard has been placed under the light of two outdoor led lamps so that the black squares became warmer than the white ones. Then, frames have been recorded for 20 different relative positions of the board. Finally, the calibration has been done with the camera calibration app of Matlab©. Vignetting has not been calibrated for this study.

$$\begin{cases} x_{DISTORTED} = x \times (1 + k_1 \times r^2 + k_2 \times r^4 + k_3 \times r^6) \\ y_{DISTORTED} = y \times (1 + k_1 \times r^2 + k_2 \times r^4 + k_3 \times r^6) \end{cases} \quad (1a)$$

$$\begin{cases} x_{DISTORTED} = x + [2 \times p_1 \times y + p_2 \times (r^2 + 2 \times x^2)] \\ y_{DISTORTED} = y + [p_1 \times (r^2 + 2 \times y^2)y + 2 \times p_2 \times x] \end{cases} \quad (1b)$$

where x and y are undistorted pixel locations, $x_{DISTORTED}$ and $y_{DISTORTED}$ are distorted pixel locations, $r^2 = x^2 + y^2$, k_1, k_2 and k_3 are the radial distortion coefficients of the lens and p_1 and p_2 are the tangential ones.

Laser distance meter calibration. This calibration has been done with the method presented by Bertrand-Krajewski (2008) and 17 calibration distances (1, 3, 5, 7, 9, 11, 13, 15, 17, 19, 21, 23, 25, 27, 29, 31 and 33 m). Measured distances have been repeatedly measured (N_M times) for each calibration distance. Based on Williamson (1968), reviewed (Reed, 1989) and corrected (Reed, 1992) the method proposed by

Bertrand-Krajewski (2008) consists to numerically minimise equation 2 when $D_{R,i}$ is a linear or polynomial function (2nd or 3rd order) of $d_{M,i}$.

$$S = \sum_{i=1}^{N_{CD}} \left[\frac{1}{\sigma^2(d_{R,i})} \times \left(D_{R,i} - d_{R,i}\right)^2 + \frac{1}{\sigma^2(d_{M,i})} \sum_{j=1}^{N_M} \left(D_{M,i,j} - d_{M,i,j}\right)^2 \right] \quad (2)$$

where $d_{R,i}$ is the real (*i.e.* calibration) distance of index i (in m) among the N_{CD} (17) ones, $\sigma(d_{R,i})$ is standard uncertainty (in m), $D_{R.i}$ is the one estimated by the calibration model (in m), $d_{M,i,j}$ (in m) is the j^{th} measurement for the distance i and $D_{M,i,j}$ (in m) is the one estimated by the calibration model and $\sigma(d_{M,i})$ is the standard deviation (in m) of the N_M (1200) $d_{M,I,j}$.

2.3.2. Data processing

Data pre-processing. Raw data requires being pre-processed before further uses and calculations. For the laser distance meter, real distances need to be calculated by the inverse calibration function from the measured distances. IR data requires more effort: vignetting and distortion corrections and the transformation of pixel (signal) values to temperatures (Eq. 3).

$$T = \frac{B}{\ln\left[\frac{R}{(S - O)} + F\right]} - 273.15 \quad (3)$$

where T is the temperature (in °C), B, R, O and F are Planck constants, which derive from the factory thermal calibration of each individual infrared camera, and S is the 14bit digital signal value.

Data conversion. With corrected data, two kinds of end-user data have been created: *i)* grey and blue-red scale videos and *ii)* 2D temperature maps. Initially scaled for the full temperature range (from - 25 °C to 135 °C), the range has been rescaled from the minimal to the maximal recorded temperatures to increase the image/video readability.

The creation of end-user friendly videos did not require any specific method except the rescaling. Figure 5 shows the rescaling effect and highlights the need of end-user adapted temperature scale.

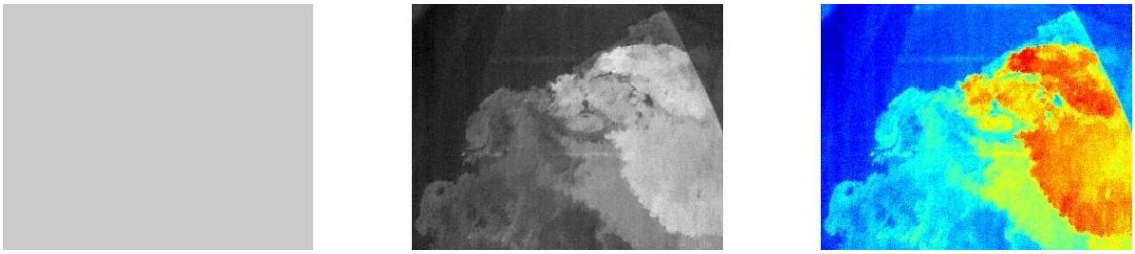

Figure 5. Plot of the frame. Full scale on the left, after temperature rescaling in the middle and after blue-red rescaling on the right. Discharge in the flume 100 l/s (15.9°C) and a lateral discharge of 2.84l/s (33.5°C) coming through the connection D 200mm.

The creation of the 2D maps has required laser data, the camera position and orientation and the post-synchronisation of both data acquisition systems.

The correspondence between the horizontal plane of the flume and the acquired frames has been achieved by taking into account the camera's spatial position along the flume (in the middle, at 45° with respect to the longitudinal axes of the flume) and the angular view of the camera (vertical 39° and horizontal 48°, manufacturer data). The design of the maps is based on the translation of the camera's resolution (256x320) to a square grid of 1x1mm, followed by the assumption that the water level is steady within the spatial range of measurements.

The camera was set to record at 60 frames per second, resulting in acquiring temperature values in numerous frames for the same positions in the flume. During the creation of the maps every square in the grid is depicted with the average of these temperature values. The outcome of this method is the improvement of the produced visualisations of the water surface, as the vignetting effect and other external factors that may introduce noise (*i.e.* the reflection of the ceiling lights) are up to a point reduced.

2.3.3. Detection of lateral connections

The detection of foreign bodies in the flume is based on the thermal differences that exist between consecutive frames in the acquired videos. Through the formed cloud, the possible perturbation due to the lateral connection can be detected with a variance test: if equation 4 is not satisfied, the temperature of the pixel is significantly different from frame to frame.

$$|T_i - T_{i-1}| \leq 2 \times \left(\sigma(T_i) + \sigma(T_{i-1})\right) \quad (4)$$

where T_i (°C), and T_{i-1} (°C), are the respective temperatures of a pixel during the experiment in two consecutive frames; and where $\sigma(T_i)$ and $\sigma(T_{i-1})$ are their standard uncertainties (°C). Figure 6 depicts different frames of the same experiment, indicating how the different type of water is tracked by the developed algorithm, based on the application of equation 4.

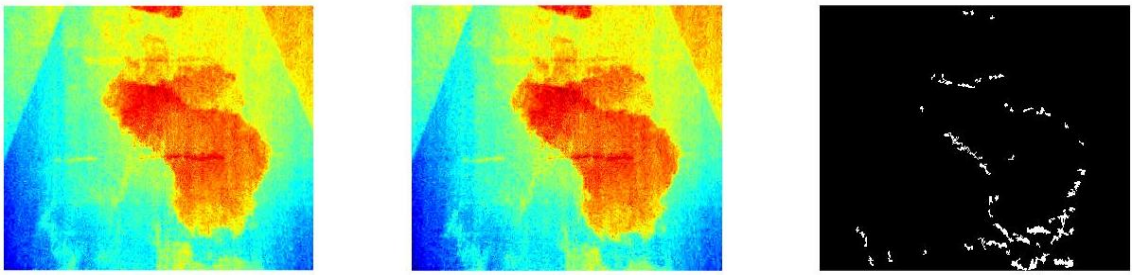

Figure 6. Plots of two consecutive frames on the left and in the middle, and the binary image of the difference after applying equation 4 on the right. Discharge in the flume 200 l/s (15.9°C) and a lateral discharge of 2.47l/s (27.5°C) coming through the connection WL 400mm.

In order to avoid detection of artefacts, a lateral connection has been considered as detectable if there is a difference in the thermal status of at least 9 grouped pixels within the range of 60 consecutive frames. These values arose after testing several combinations on experiments that presented intense effects of artefacts (i.e. the reflection of the ceiling lights), and were afterwards applied to the whole range of experiments.

2.3.4. Quantification of lateral connections

While considering water masses along the reach (the lateral connection and the pipe: upstream and downstream) and due to the high frequency of the IR camera (60 fps), the system can be considered as adiabatic. Right at the lateral connection, no other external source or well of energy may affect the temperature distribution at the free surface. This is a strong simplifying assumption but the following balance can be written (Eq. 5):

$$Q_{LC} \times T_{LC} + Q_U \times T_U = Q_D \times T_D \quad (5)$$

where Q_{LC}, Q_U and respectively Q_D are the discharges (m^3/s) of the lateral connection, the main pipe upstream and respectively downstream of the lateral connection with their respective temperatures (T_{LC}, T_U and T_D in °C).

While assuming no leakage and no other lateral connection, equation 5 can be re-written as following (Eq. 6).

$$Q_{LC} \times T_{LC} + Q_U \times T_U = (Q_{LC} + Q_U) \times T_D \quad (6)$$

And Q_{LC} is finally calculated (Eq. 7).

$$Q_{LC} = Q_U \times \frac{T_D - T_U}{T_{LC} - T_D} \quad (7)$$

Three ways may be used to estimate T_{LC}: *i)* a direct measurement of the temperature with IR image if the connection is above the water level (water fall), *ii)* estimation of the maximal or minimal values with IR data if the connection is below the water level (the real temperature is equal or colder, and respectively equal or warmer, than the minimal or maximal value at the free surface for cold, and respectively warm, lateral connections) and *iii)* estimation by other measurements or estimations (as for temperatures of ground water tables). In case the second way is applied, the discharge from the lateral connection can be delimited as following (Equation 8, for cold lateral

connection and Equation 9 for warm lateral connection):

$$Q_{LC} \geq Q_U \times \frac{T_D - T_U}{T_{LC,EST-COLD} - T_D} \quad (8)$$

$$Q_{LC} \leq Q_U \times \frac{T_D - T_U}{T_{LC,EST-WARM} - T_D} \quad (9)$$

where $T_{LC,EST-COLD}$, and respectively, $T_{LC,EST-WARM}$ are the estimated temperatures (°C) of the cold, and respectively warm, lateral connections assuming to be equal to the minimal, and respectively the maximal, temperature of the free surface.

The application of the law of uncertainty propagation to equation 7 led to the estimation of the standard uncertainty of the lateral connection (Eq. 10).

$$\sigma(Q_{LC}) = \sqrt{\begin{array}{c} \sigma^2(Q_U) \times \left(\frac{T_D - T_U}{T_{LC} - T_D}\right)^2 + \sigma^2(T_U) \times \left(\frac{Q_U}{T_{LC} - T_D}\right)^2 \\ +\sigma^2(T_D) \times \left(\frac{Q_U \times (T_{LC} - T_U)}{(T_{LC} - T_D)^2}\right)^2 + \sigma^2(T_{LC}) \times \left(\frac{Q_U \times (T_D - T_U)}{{T_{LC}}^2}\right)^2 \\ +2 \times cov(T_U, T_D) \times \left(\frac{Q_U}{T_{LC} - T_D}\right) \times \left(\frac{Q_U \times (T_{LC} - T_U)}{(T_{LC} - T_D)^2}\right) \\ +2 \times cov(T_U, T_{LC}) \times \left(\frac{Q_U}{T_{LC} - T_D}\right) \times \left(\frac{Q_U \times (T_D - T_U)}{{T_{LC}}^2}\right) \\ +2 \times cov(T_D, T_{LC}) \times \left(\frac{Q_U \times (T_{LC} - T_U)}{(T_{LC} - T_D)^2}\right) \times \left(\frac{Q_U \times (T_D - T_U)}{{T_{LC}}^2}\right) \end{array}} \quad (10)$$

where $\sigma(Q_U)$ (in m^3/s) is the standard uncertainty on Q_U, $\sigma(T_U)$ (in °C) is the standard uncertainty on T_U, $\sigma(T_{LC})$ (in °C) is the standard uncertainty on T_{LC}, $\sigma(T_D)$ (in °C) is the standard uncertainty on T_D (Table 3) and under the assumption that there is no correlation between the temperatures (T_{LC}, T_U and T_D) and the discharge upstream the lateral connection.

Since T_U and T_D are measured in the same pipe, by the same camera connected to the same data acquisition system, $cov(T_U,T_D)$ is assumed to be equal to $\sigma(T_U).\sigma(T_D)$. Depending on how is T_{LC} measured or estimated, equation 10 is finally simplified to

equation 11a, and respectively equation 11b, when the T_{LC} is estimated or measured with IR data, and respectively with another way.

$$\sigma(Q_{LC}) = \sqrt{\begin{array}{c} \sigma^2(Q_U) \times \left(\frac{T_D - T_U}{T_{LC} - T_D}\right)^2 + \sigma^2(T_U) \times \left(\frac{Q_U}{T_{LC} - T_D}\right)^2 \\ +\sigma^2(T_D) \times \left(\frac{Q_U \times (T_{LC} - T_U)}{(T_{LC} - T_D)^2}\right)^2 + \sigma^2(T_{LC}) \times \left(\frac{Q_U \times (T_D - T_U)}{{T_{LC}}^2}\right)^2 \\ +2 \times \left(\frac{Q_U}{T_{LC} - T_D}\right) \times \left(\frac{Q_U \times (T_{LC} - T_U)}{(T_{LC} - T_D)^2}\right) \\ +2 \times \left(\frac{Q_U}{T_{LC} - T_D}\right) \times \left(\frac{Q_U \times (T_D - T_U)}{{T_{LC}}^2}\right) \\ +2\left(\frac{Q_U \times (T_{LC} - T_U)}{(T_{LC} - T_D)^2}\right) \times \left(\frac{Q_U \times (T_D - T_U)}{{T_{LC}}^2}\right) \end{array}} \quad (11a)$$

$$\sigma(Q_{LC}) = \sqrt{\begin{array}{c} \sigma^2(Q_U) \times \left(\frac{T_D - T_U}{T_{LC} - T_D}\right)^2 + \sigma^2(T_U) \times \left(\frac{Q_U}{T_{LC} - T_D}\right)^2 \\ +\sigma^2(T_D) \times \left(\frac{Q_U \times (T_{LC} - T_U)}{(T_{LC} - T_D)^2}\right)^2 + \sigma^2(T_{LC}) \times \left(\frac{Q_U \times (T_D - T_U)}{{T_{LC}}^2}\right)^2 \\ +2 \times cov(T_U, T_D) \times \left(\frac{Q_U}{T_{LC} - T_D}\right) \times \left(\frac{Q_U \times (T_{LC} - T_U)}{(T_{LC} - T_D)^2}\right) \end{array}} \quad (11b)$$

The discharge coming from the lateral connection and calculated by equation 7 is finally compared to the known discharge ($Q_{LC,TRUE}$) calculated with the difference in the water levels in the tank and the duration of the opening of the valve (Eq. 12a) and its standard uncertainty (Eq. 12b, Table 3).

$$Q_{LC,TRUE} = \frac{A_{TANK} \times (h_{BEGINNING} - h_{END})}{d} \quad (12a)$$

$$\sigma(Q_{LC,TRUE}) = \sqrt{\begin{array}{c} \sigma^2(A_{TANK}) \times \left[\frac{(h_{BEGINNING} - h_{END})}{d}\right]^2 \\ +\left(\frac{A_{TANK}}{d}\right)^2 \times \left(\sigma(h_{BEGINNING}) - \sigma(h_{END})\right)^2 \\ +\sigma^2(d) \times {A_{TANK}}^2 \times (h_{BEGINNING} - h_{END})^2 \end{array}} \quad (12b)$$

Due to the fact that Q_{LC} and $Q_{LC,TRUE}$ are estimated by two completely independent methods, the lateral connection is considered as quantifiable if the equation 13 is satisfied.

$$\left|Q_{LC} - Q_{LC,TRUE}\right| \leq 2 \times \sqrt{\sigma^2(Q_{LC}) + \sigma^2\left(Q_{LC,TRUE}\right)} \quad (13)$$

Table 3. List of the used values of standard uncertainties

$\sigma(A_{TANK})$ (m2)	σ(d) (s)	$\sigma(h_{BEGINNING})$ (m)	$\sigma(h_{END})$ (m)	$\sigma(T_D)$ (°C)	$\sigma(T_{LC})$ (°C)	$\sigma(T_U)$ (°C)
0.05	0.3	0.005	0.005	0.01	0.05	0.01

3. Results

3.1. Sensor calibrations

The laser distance meter offers a good linearity: the straight-line function has been retained (Fig. 7) by a Fischer-Snedector test.

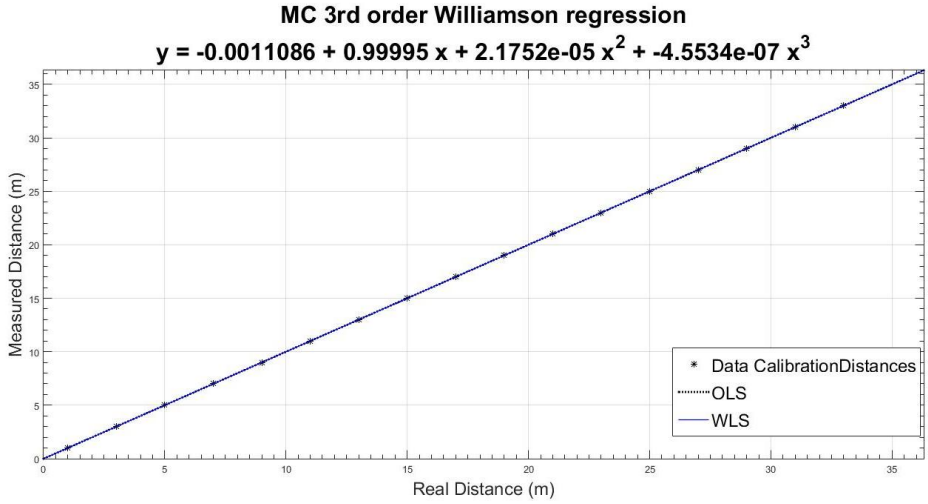

Figure 7. Function of the measured and real distances

The distortion calibration with the camera calibration app of Matlab© generated a parameters set (Table 4) which takes into consideration the known intrinsic

characteristics of the camera and can be applied to any image recorded by the specific camera. Figure 8 shows the end result in a random frame of the flume.

Table 4. List of the calibration coefficients according to Eq.1

Radial Coefficients			Tangential Coefficients	
k_1 (-)	k_2 (-)	k_3 (-)	p_1 (-)	p_2 (-)
0.438	0.143	0.171	-5.228 e-4	0.002

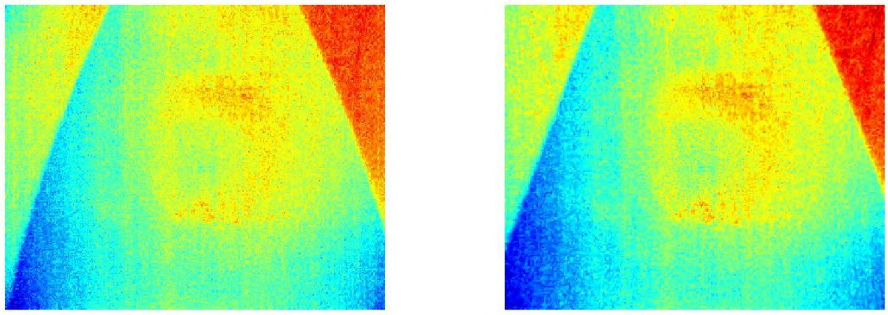

Figure 8. Image before (left) and after (right) distortion calibration: the perspective lines (water, glass window) are straight on the right picture.

3.2. Detection and quantification limits of the proposed methods

Based on the experiments and the methods previously described, experiments present three possible results. The lateral connection is *i)* not detectable, *ii)* detectable but not quantifiable and *iii)* quantifiable.

Figures 9, 10, 11 and 12 depict the ability of the proposed methods to detect leaking lateral connections. These graphs consist of 3 axes: in the x axis the temperature ratio of the examined connection and the flume, in the y axis the discharge ratio of the examined connection and the flume, and in the z axis the ratio between the distance of the lateral connection with the invert level of the flume and the water level in the flume. Additionally, there are two planes: the red plane which discriminates the water type of the connection (warm/cold), and the green plane which indicates the experiments in

which the top part of the lateral connection was above the water depth. Based on the hydraulic conditions, the various Reynolds Numbers are incorporated in the graphs according to the size of the markers (the smallest marker corresponds to Re equal to 150000 and the largest one to 850000).

The connection is depicted with a filled marker (if detectable), whereas non-detectable connections are presented with empty markers.

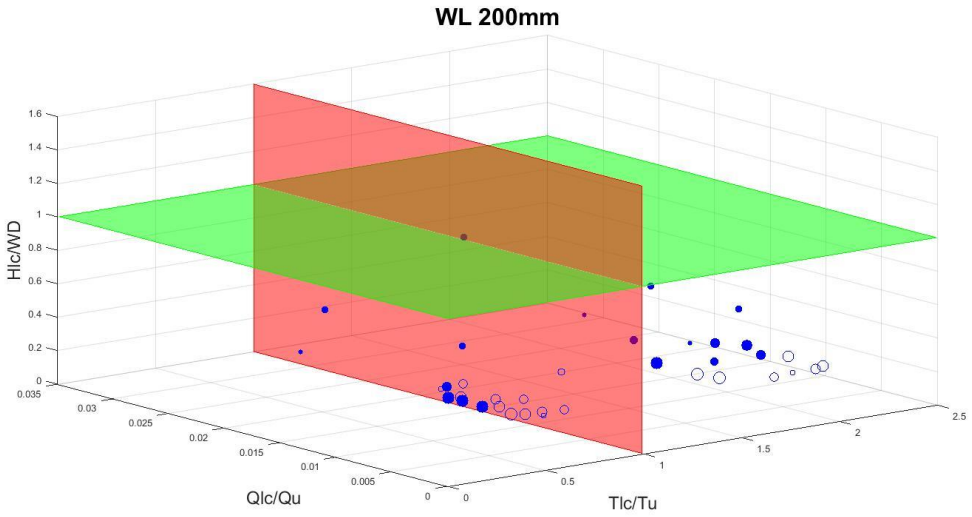

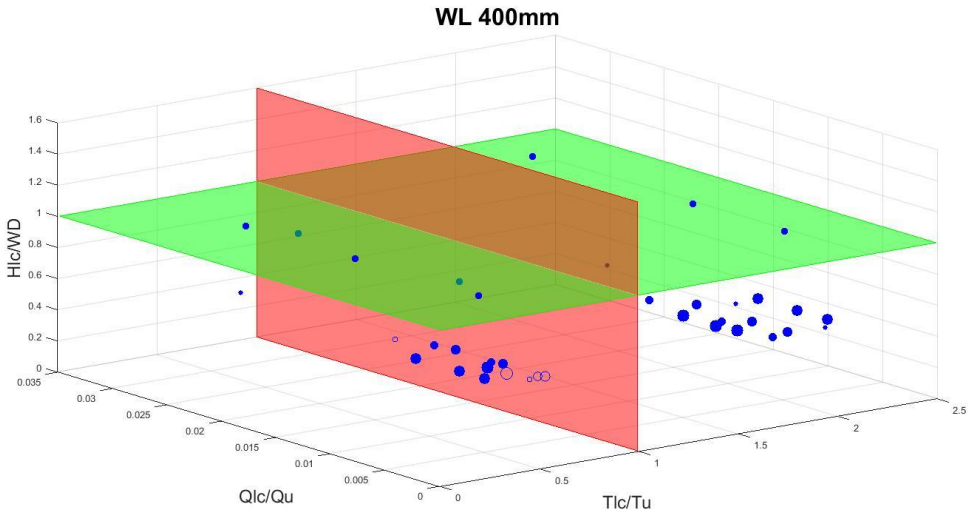

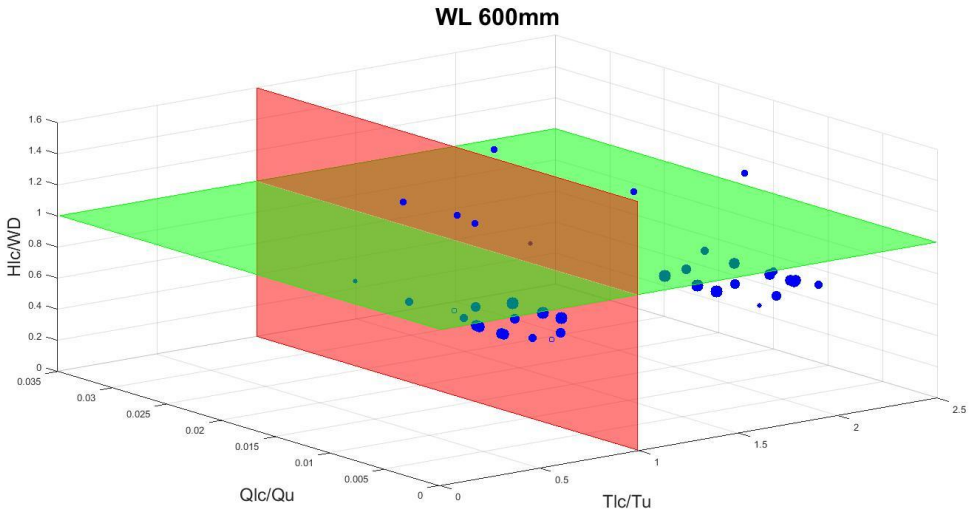
WL 600mm
Hlc/WD
Qlc/Qu
Tlc/Tu

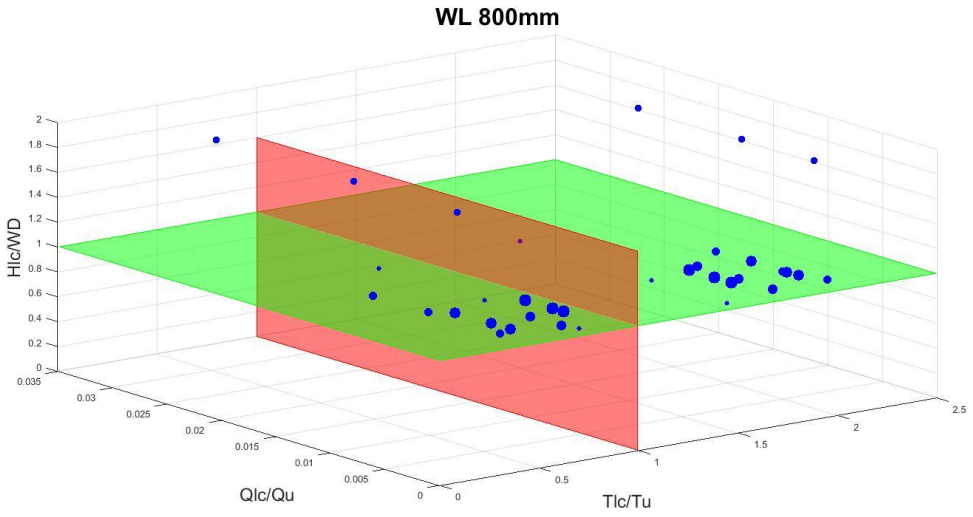
WL 800mm
Hlc/WD
Qlc/Qu
Tlc/Tu

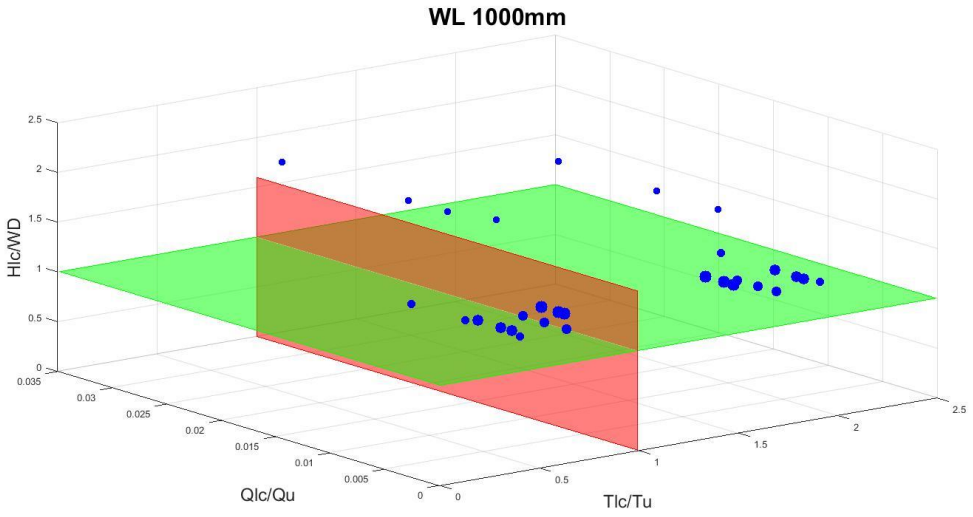
WL 1000mm
Hlc/WD
Qlc/Qu
Tlc/Tu

Figure 9. 3D scatter plots of detection capability for connections: a) WL 200 mm b) WL 400 mm c) WL 600 mm d) WL 800 mm e) WL 1000 mm. The filled markers are the detected connections. The T_{LC}/T_U and Q_{LC}/Q_U are the temperature and discharge ratios between the lateral connection and the flume respectively. The H_{LC}/WD indicates the position of the lateral connection with respect to the water level.

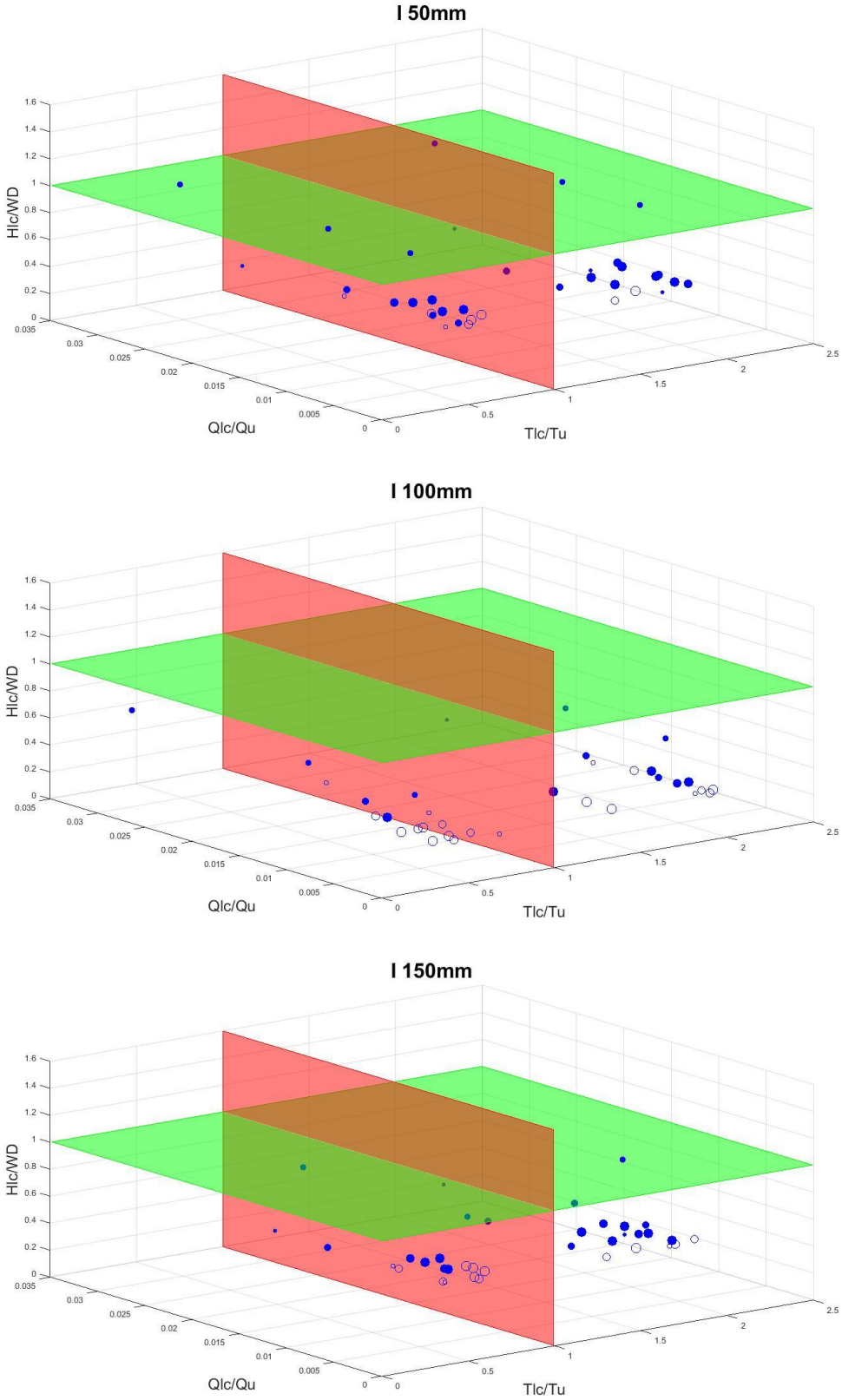

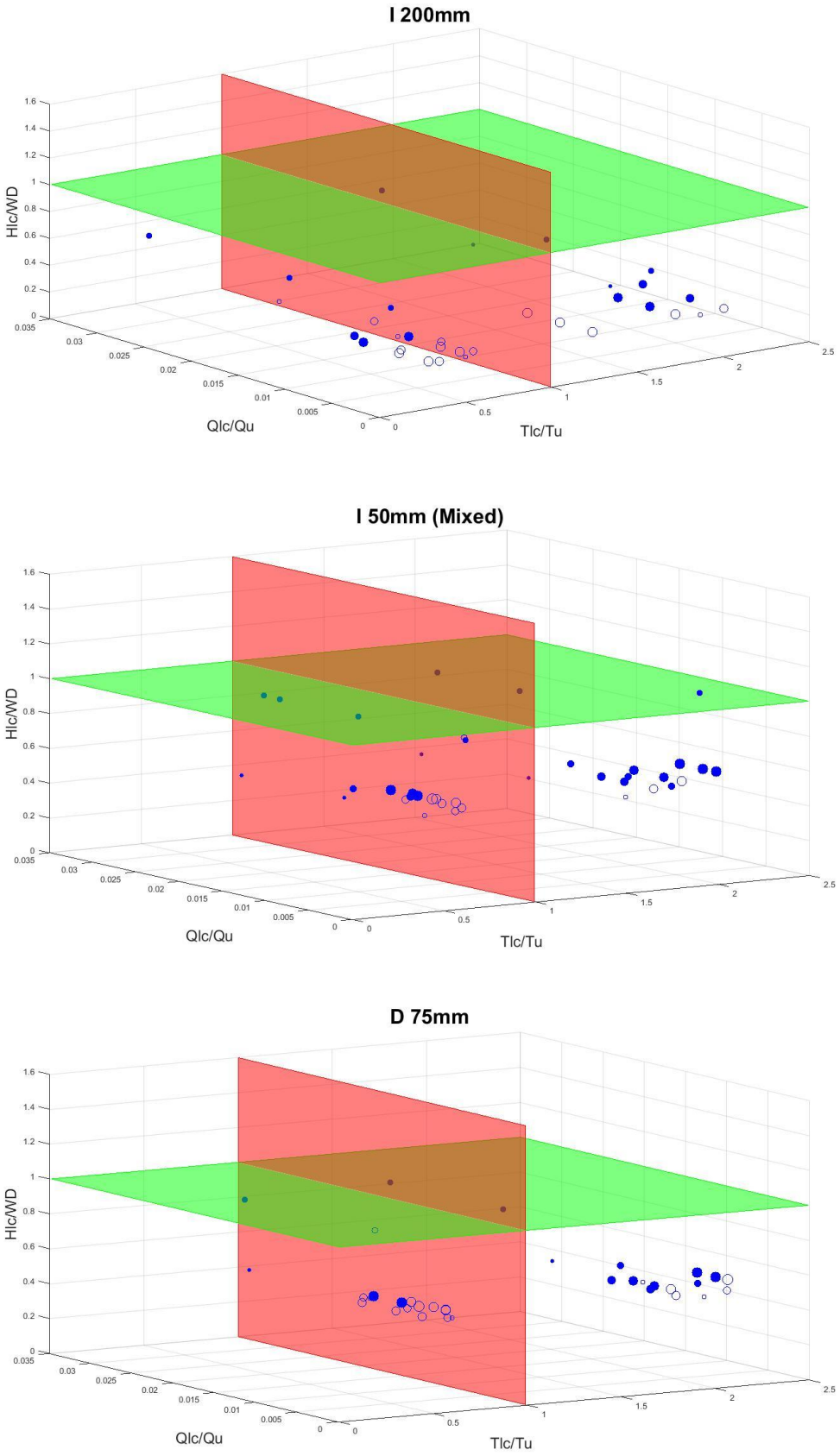

Figure 10. 3D scatter plots of detection capability for connections: a) I 50 mm b) I 100 mm c) I 150 mm d) I 200 mm e) I 50 mm (Mixed) f) D 75mm. The filled markers are the detected connections. The T_{LC}/T_U

and Q_{LC}/Q_U are the temperature and discharge ratios between the lateral connection and the flume respectively. The H_{LC}/WD indicates the position of the lateral connection with respect to the water level.

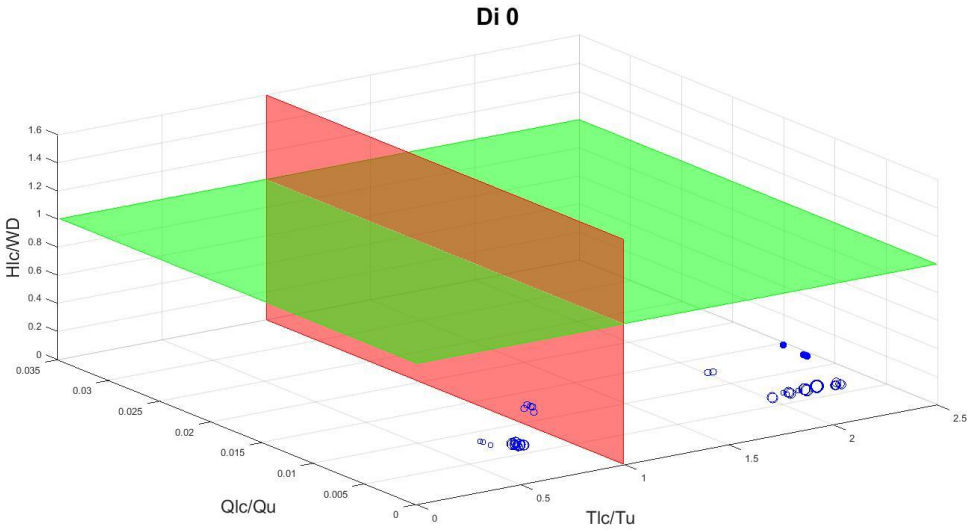

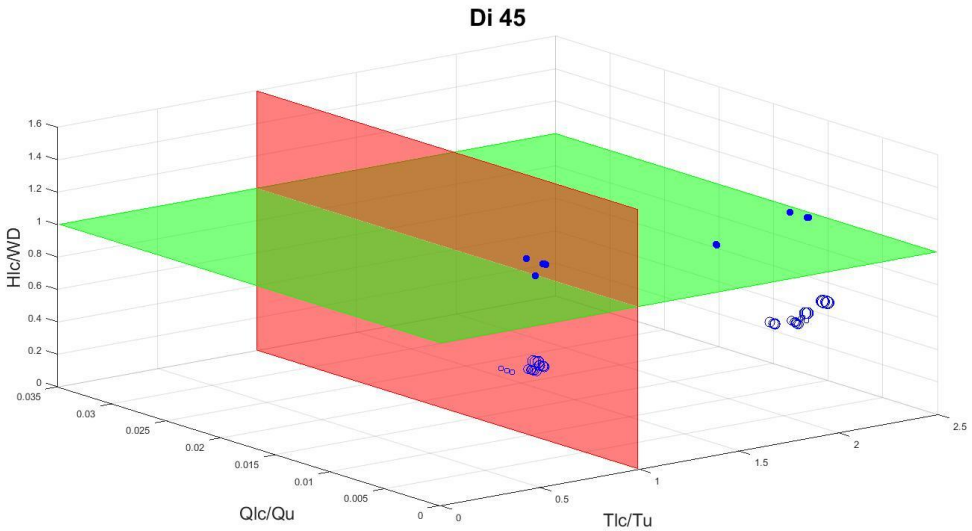

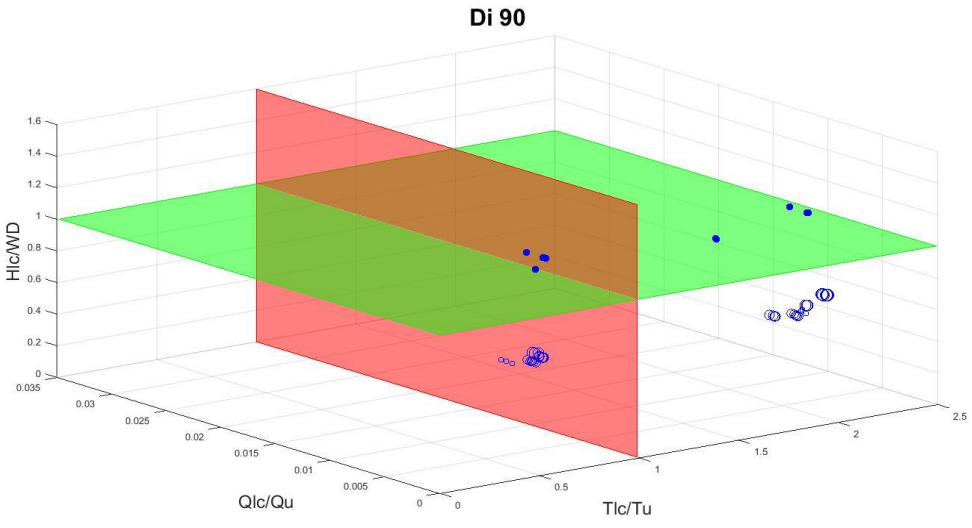

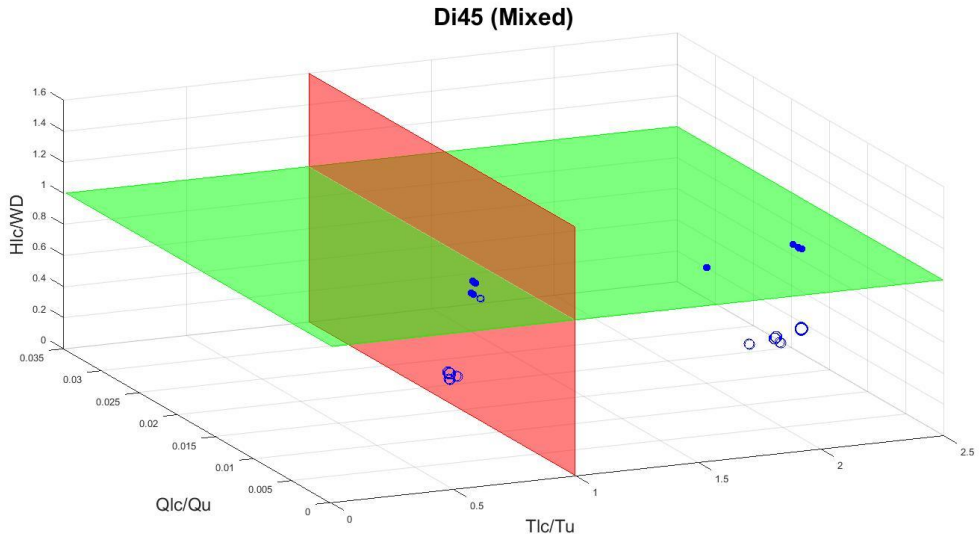

Figure 11. 3D scatter plots of detection capability for connections: a) Di 0 b) Di 45 c) Di 90 d) Di-45 (Mixed). The filled markers are the detected connections. The T_{LC}/T_U and Q_{LC}/Q_U are the temperature and discharge ratios between the lateral connection and the flume respectively. The H_{LC}/WD indicates the position of the lateral connection with respect to the water level.

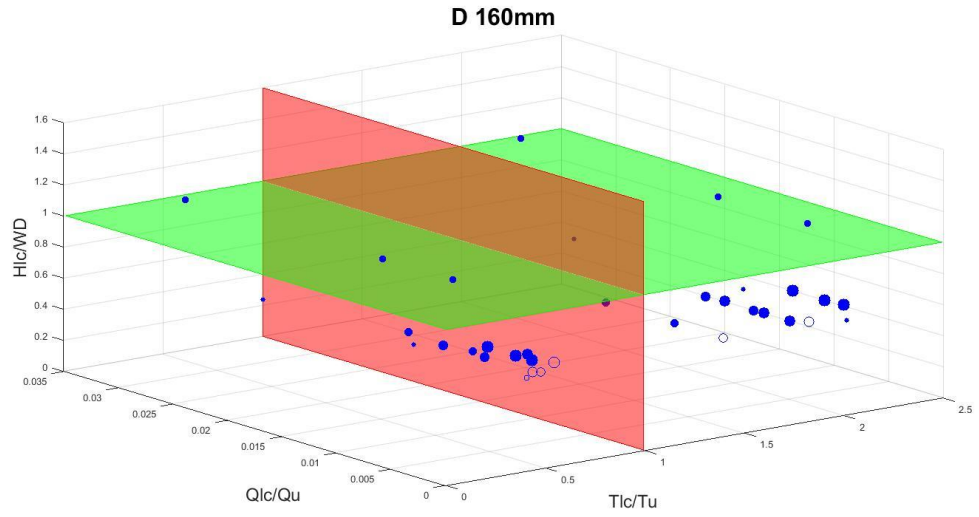

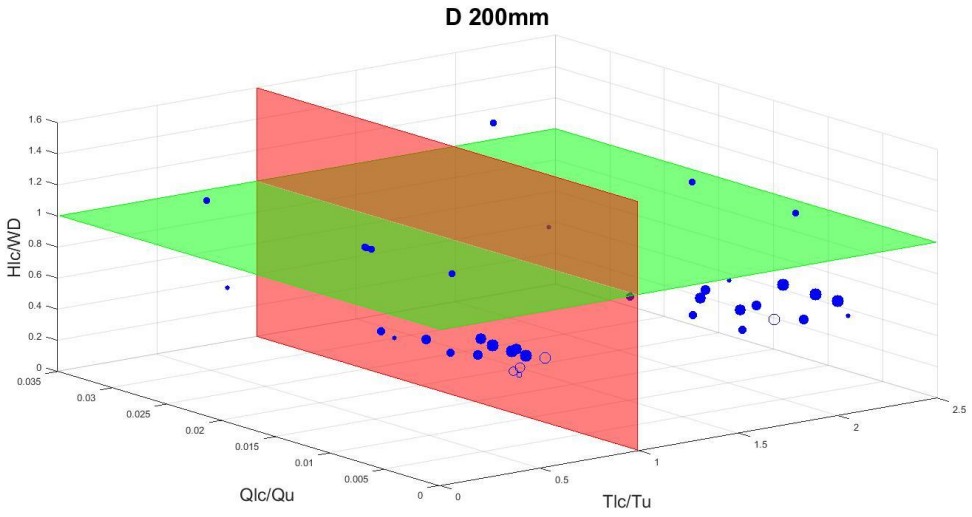

Figure 12. 3D scatter plots of detection limits for connections: a) D160 mm b) D 200 mm. The filled markers are the detected connections. The T_{LC}/T_U and Q_{LC}/Q_U are the temperature and discharge ratios between the lateral connection and the flume respectively. The H_{LC}/WD indicates the position of the lateral connection with respect to the water level.

The experiments that were signed as "detectable connections" were further processed in order to examine their quantification. An important step to achieve this is the creation of the 2D temperature maps of the free surface and the respective graphs of the average temperature along the flume, which are derived by the maps. Figure 13 present two examples of maps with different types of water that were used at this process.

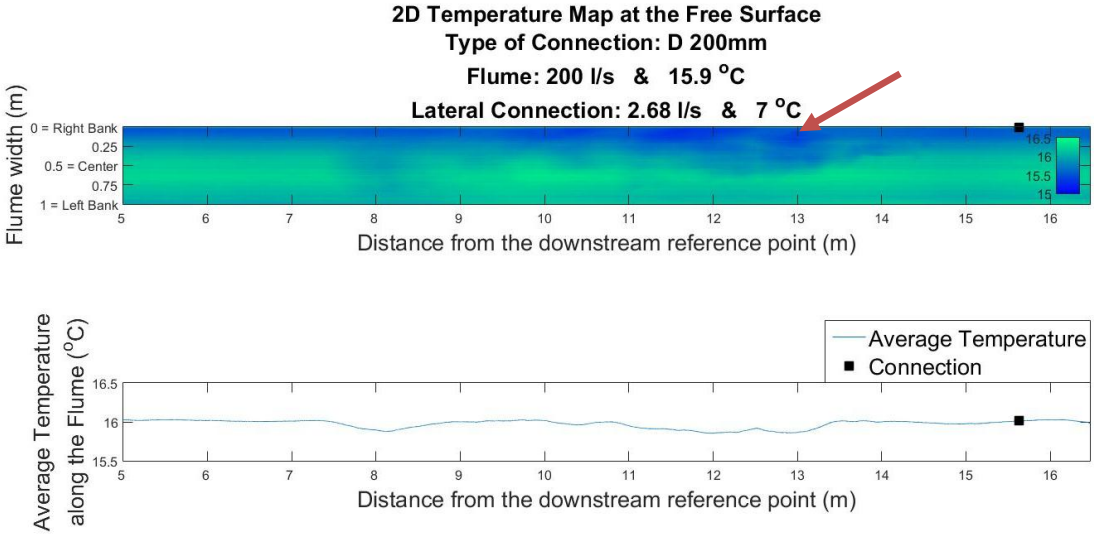

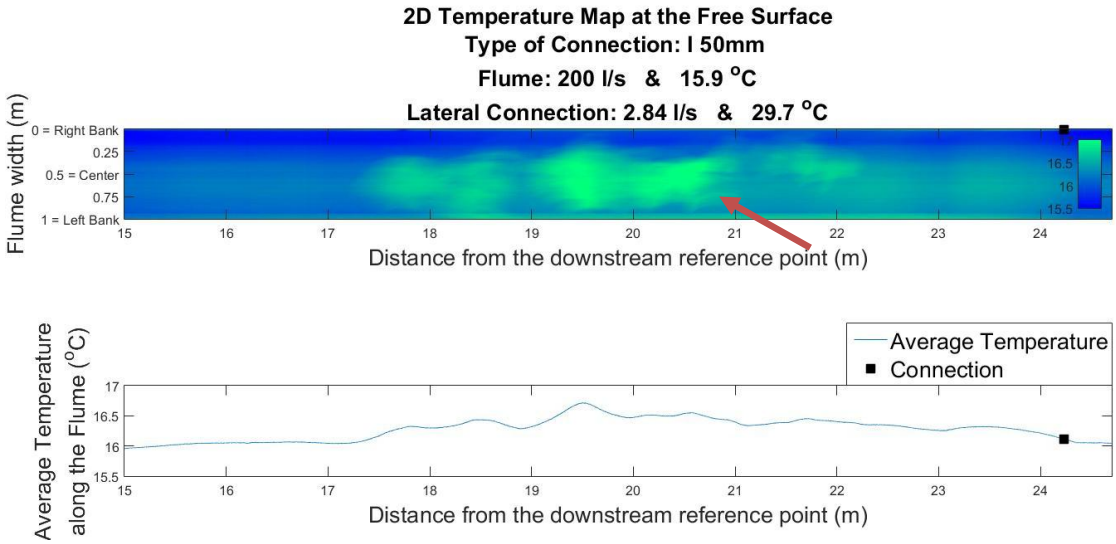

Figure 13. 2D temperature Maps of the free surface with their respective graphs of the average temperature. The top map is for a cold lateral connection and the bottom map is for a warm one. The arrays indicate the effect of the lateral connection.

By using this type of figures to select the T_U and T_D, and track the T_{LC}, the equations presented in section 2.3.4 were used, leading to results regarding the quantification of the tested, detectable connections. Figures 14, 15, 16 and 17 show the ability of the proposed method to quantify. In the x axis it is the temperature ratio of the examined connection and the flume, and in the y axis it is the ratio between the estimated discharge of the lateral connection that came from the IR measurements and the real discharge. The y axis is in log scale in order to avoid skewness caused by large values, leading to the omitting of negative values. The green line exists to discriminate between the types of water, whereas the red line exists as a reference of the desired results.

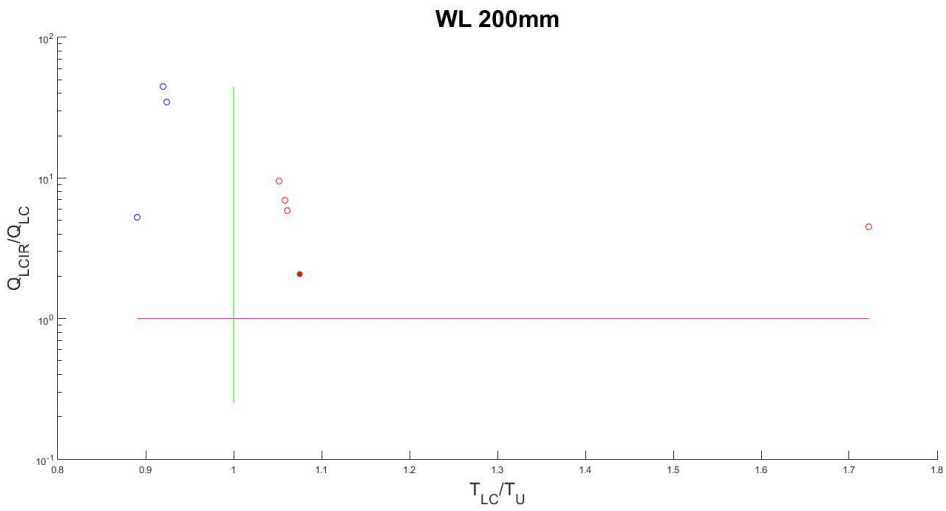
WL 200mm
Q_{LCIR}/Q_{LC}
T_{LC}/T_U

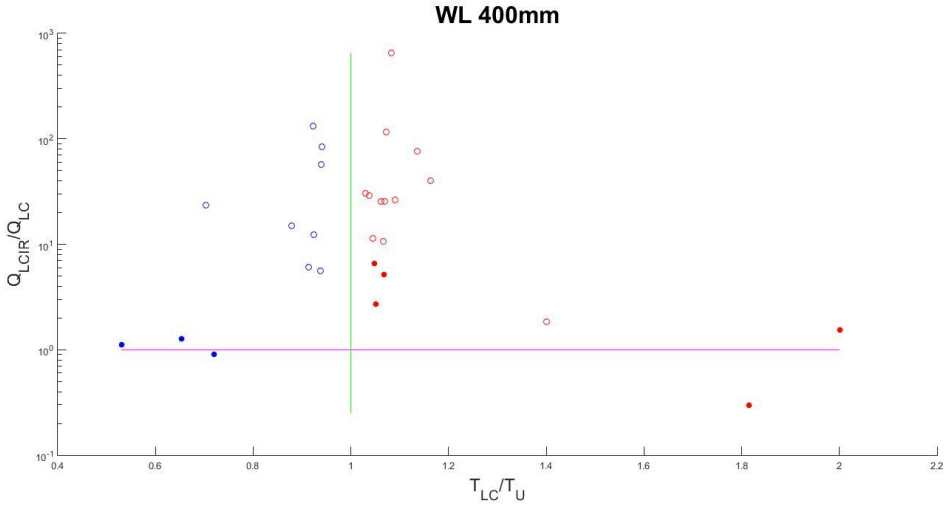
WL 400mm
Q_{LCIR}/Q_{LC}
T_{LC}/T_U

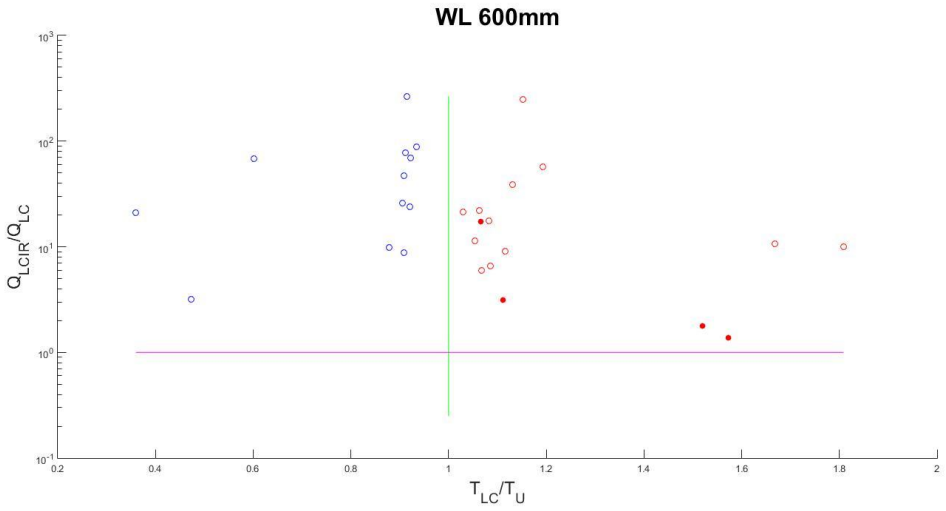
WL 600mm
Q_{LCIR}/Q_{LC}
T_{LC}/T_U

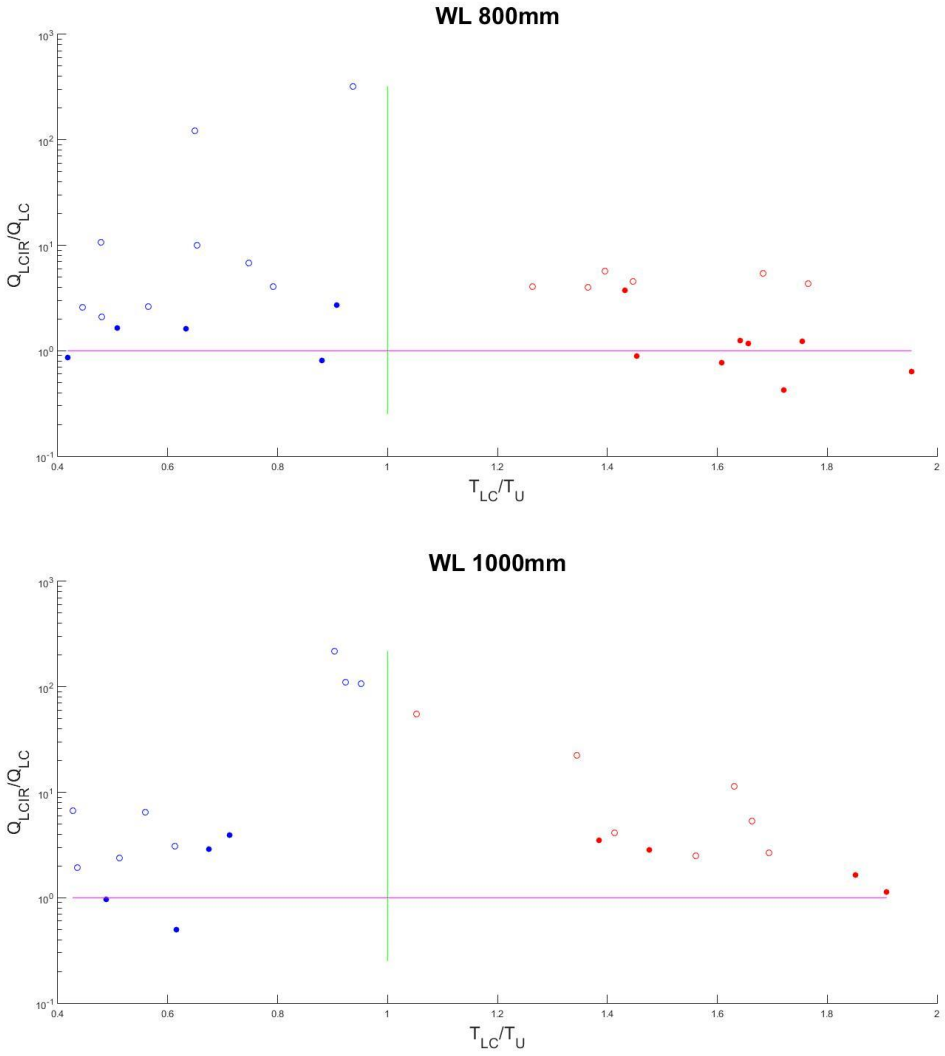

Figure 14. 2D scatter plots of quantification capability for connections: a) WL 200 mm b) WL 400 mm c) WL 600 mm d) WL 800 mm e) WL 1 000 mm. The filled markers are the quantifiable connections. The T_{LC}/T_U is the temperature ratio between the lateral connection and the flume. The Q_{LCIR}/Q_{LC} is the ratio between the estimated discharge (IR measurements) and the real discharge of the lateral connection.

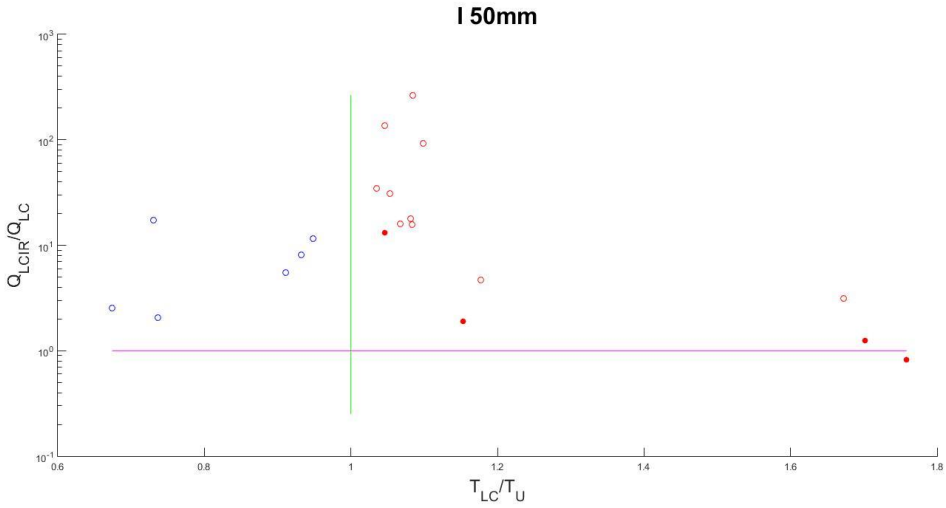
l 50mm
Q_{LCIR}/Q_{LC}
T_{LC}/T_U

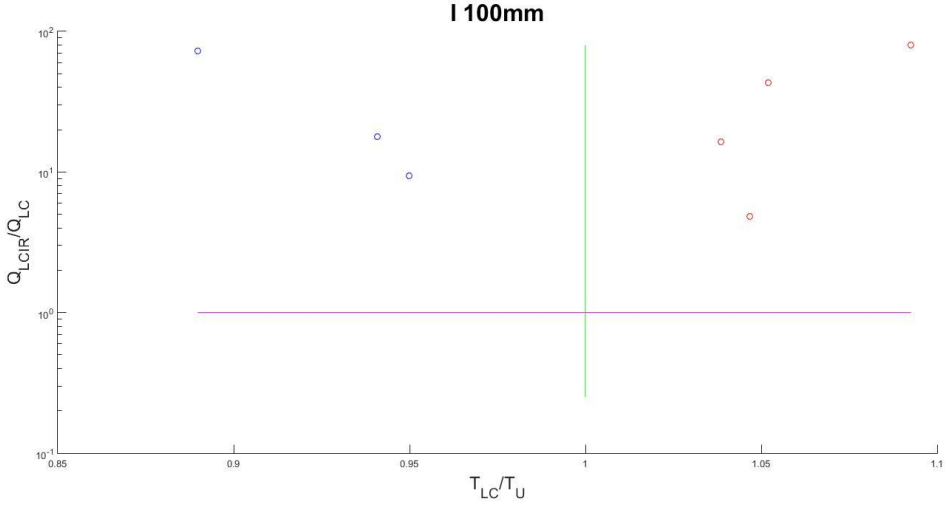
l 100mm
Q_{LCIR}/Q_{LC}
T_{LC}/T_U

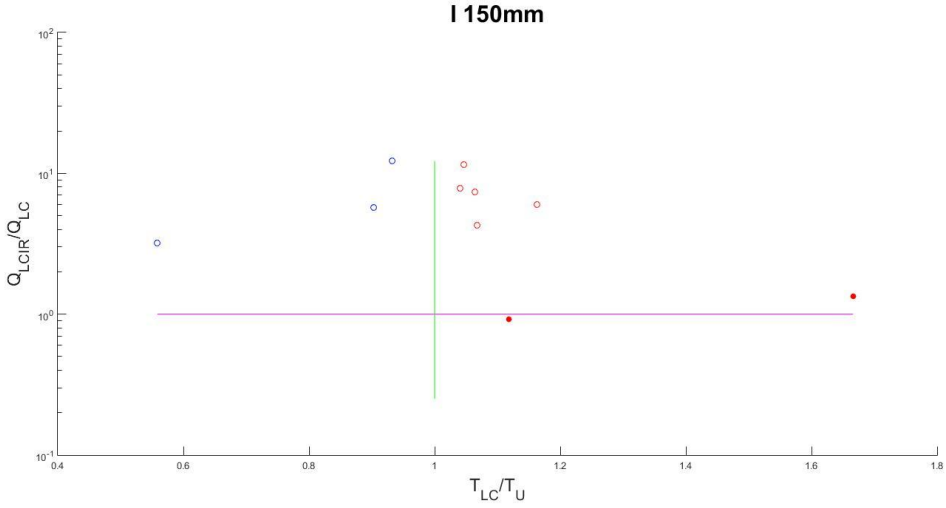
l 150mm
Q_{LCIR}/Q_{LC}
T_{LC}/T_U

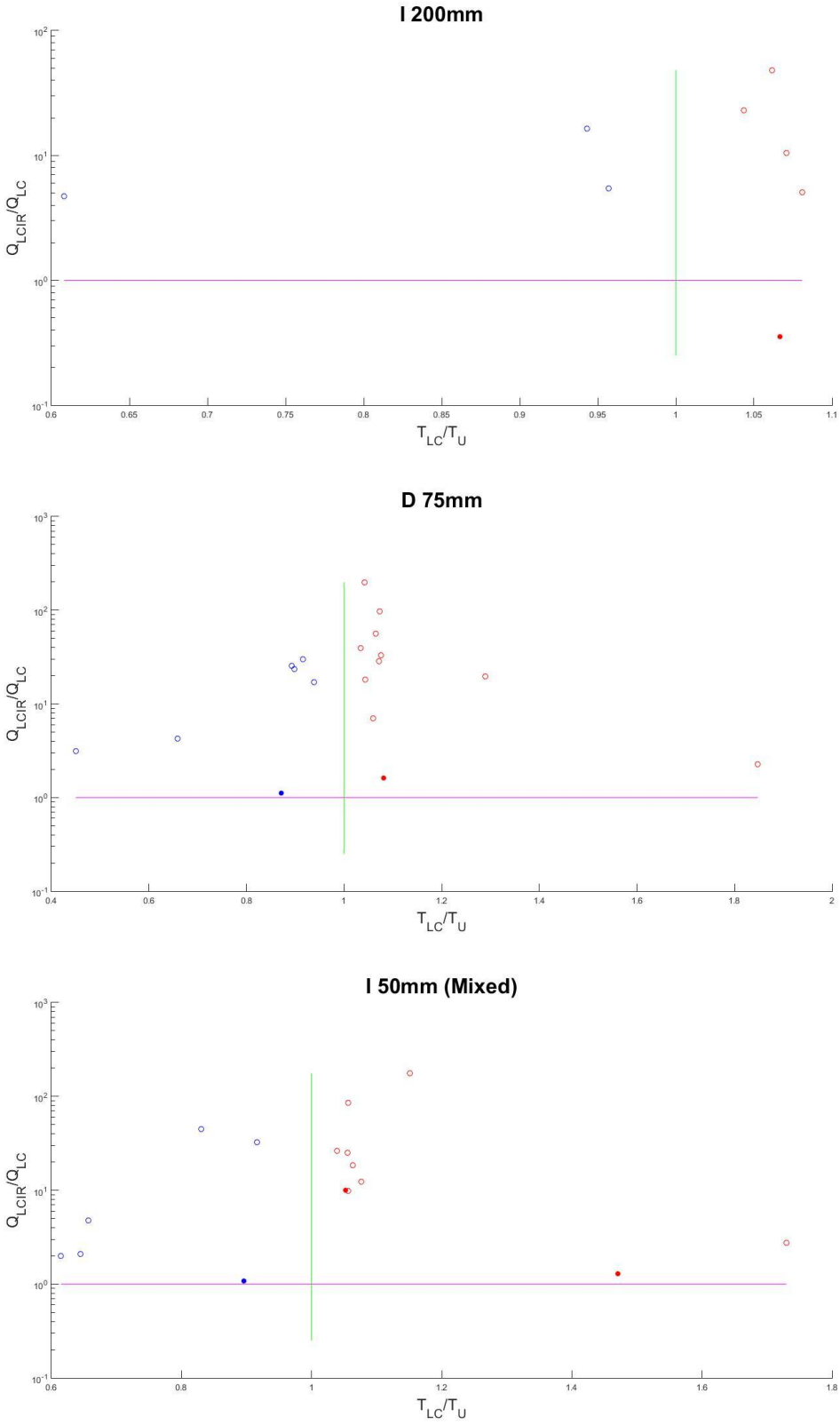

Figure 15. 2D scatter plots of quantification capability for connections: a) I 50 mm b) I 100 mm c) I 150 mm d) I 200 mm e) I 50 mm (Mixed) f) D 75mm. The filled markers are the quantifiable connections. The T_{LC}/T_U is the temperature ratio between the lateral connection and the flume. The Q_{LCIR}/Q_{LC} is the ratio between the estimated discharge (IR measurements) and the real discharge of the lateral connection.

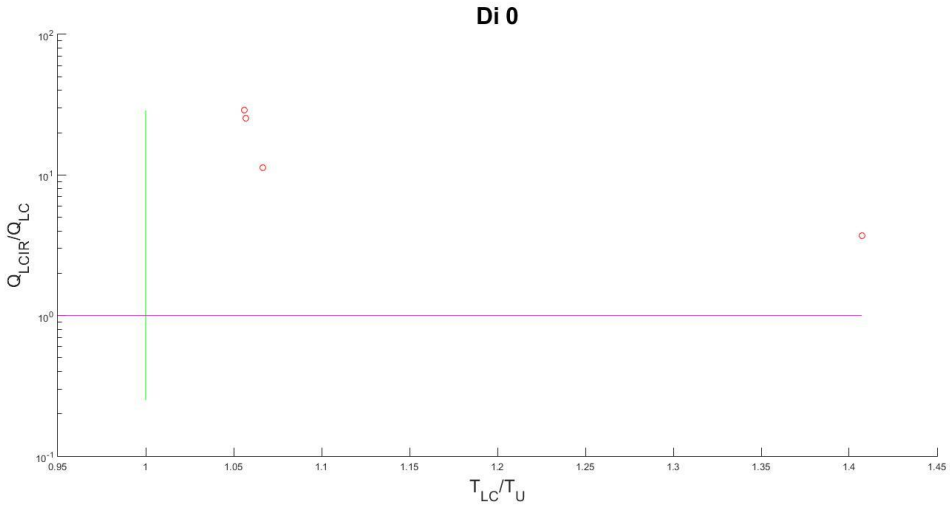
Di 0
Q_{LCIR}/Q_{LC}
T_{LC}/T_U

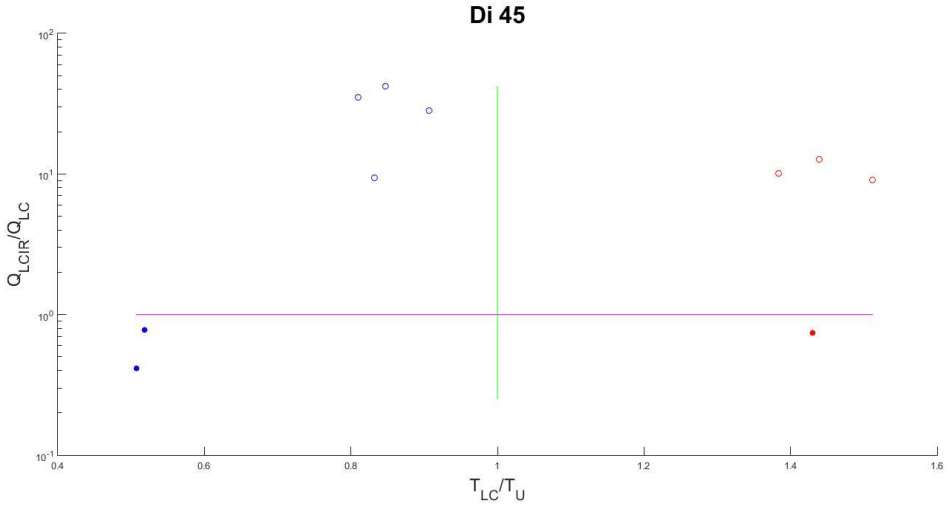
Di 45
Q_{LCIR}/Q_{LC}
T_{LC}/T_U

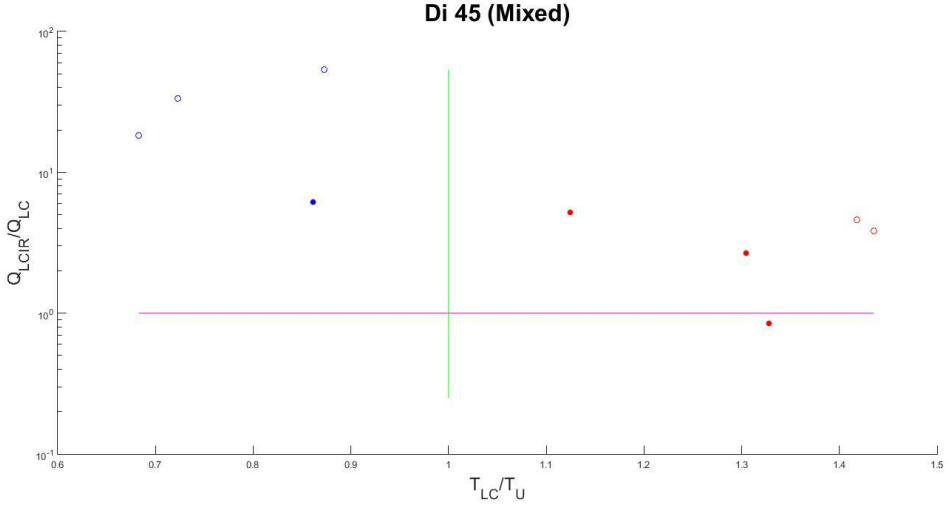
Di 45 (Mixed)
Q_{LCIR}/Q_{LC}
T_{LC}/T_U

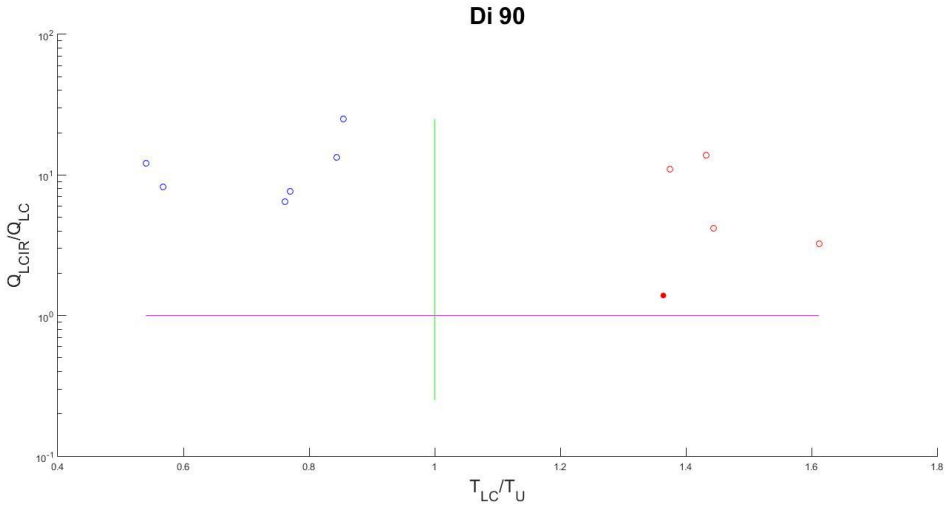

Figure 16. 2D scatter plots of quantification capability for connections: a) Di 0 b) Di 45 c) Di-45 (Mixed) d) Di 90. The filled markers are the quantifiable connections. The T_{LC}/T_U is the temperature ratio between the lateral connection and the flume. The Q_{LCIR}/Q_{LC} is the ratio between the estimated discharge (IR measurements) and the real discharge of the lateral connection.

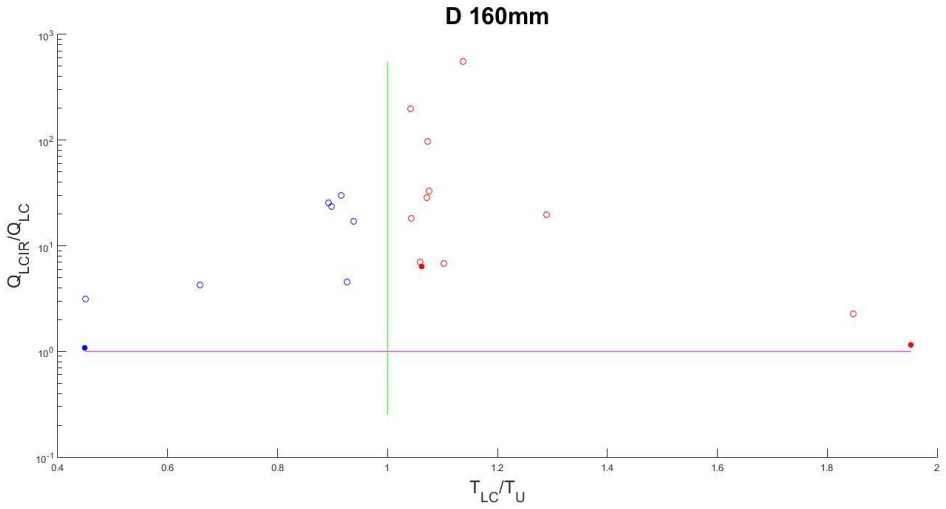

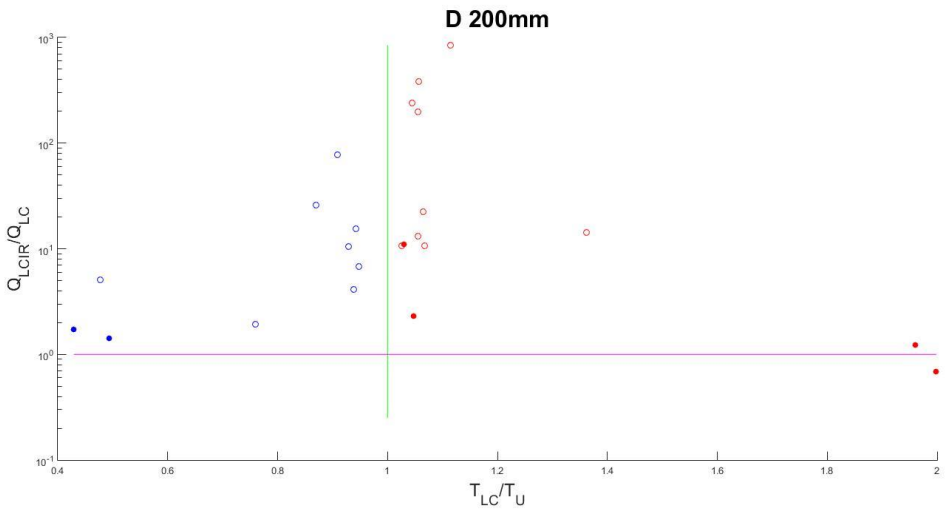

Figure 17. 2D scatter plots of quantification capability for connections: a) D160 mm b) D 200 mm. The filled markers are the quantifiable connections. The T_{LC}/T_U is the temperature ratio between the lateral connection and the flume. The Q_{LCIR}/Q_{LC} is the ratio between the estimated discharge (IR measurements) and the real discharge of the lateral connection.

4. Discussion

4.1. Parameters affecting the detection

The initial aim of the research was to identify the detection and quantification limits, leading to contour plots that clearly indicate whether an illicit lateral connection exists and its discharge, given the discharge in the system and the data acquired by the IR camera. However, despite the large number of experiments, that is not feasible, for two main reasons: *i)* a lack of information for values of the ratio $T_{LC}/T_{U,}$ which are closer to 1, and *ii)* no clear tendency is visible in the previously plotted graphs (no clear area with filled and non-filled markers).

The obtained results appear to be rather independent from the Reynolds number: several values of the Reynolds Number have been implemented during the experiments, in order to simulate various hydraulic conditions. Nevertheless, these values are achieved by adjusting the pumping flow and the downstream boundary condition, resulting in different water levels. That fact in combination with the stationary position of the connections for all the experiments makes it scientifically arbitrary to actually correlate the results with the Reynolds Number. However, what seems to be crucial is the level of the connection with respect to the water level in the flume. The deeper connections are more difficult to be detected. Further experiments with a finer tune of flume (to do experiments while varying only the water level or the Reynolds number) are needed to enhance those preliminary conclusions.

As expected, the higher is the Q_{LC}/Q_U ratio the better is the detection. However, in order to reach low values of this ratio, the discharge in the flume was increased, resulting in some extra noise in the IR frames (Fig 18): a factor that may have affected the detection.

Finally, there is a stronger tendency to detect connections that provide warm type of water than cold, which is expected if the density differences due to the temperature are taken into consideration. It is also obvious that it is almost impossible to detect the introduced water by the diffusers, which could be caused by the lower values of Q_{LC} and/or by the fact that water is introduced in a wider spatial range.

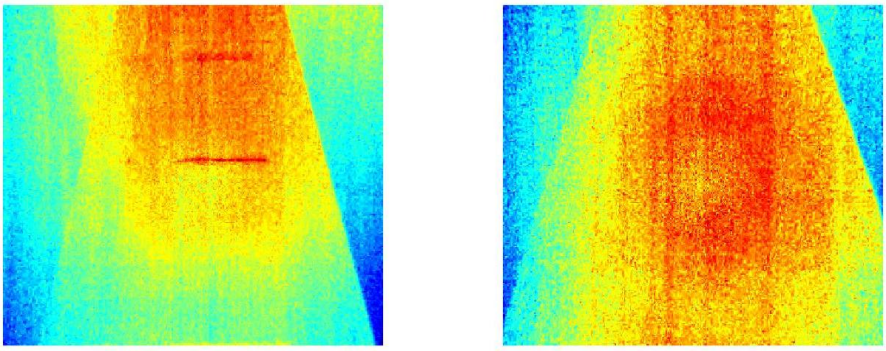

Figure 18. Extra noise due to discharge differences. Frame at Q_U=100l/s on the left and at Q_U=500l/s on the right. The focus of the camera lens is manually adjusted for every water level.

4.2. Parameters affecting the quantification

The experiments were implemented taking into account the limited quantity of warm/cold water in the tank. In addition to this, there was also a specific spatial range that the sensors train could be moved along the flume, because of connectivity issues (length of Ethernet/Usb cables). As a consequence, the IR camera tracked the foreign fluid prior to its full diffusion within the flume, as it is depicted in the presented maps. Hence, it was quite subjective the selected point along the flume at which the downstream temperature is represented since the average temperature along the flume

never presents two clear steps identifiable as T_U and T_D. Of course, this is of major importance, since this value is included in both the equations of estimating the discharge of the lateral connections (7) and of the respective uncertainties (11b). An unpredicted parameter that influences the outcome is that the measurements by the used infrared camera in many experiments suffer from inconsistencies, which is partially explained by the fact that it is an uncooled infrared camera (effects of the sensor temperature). However, the use of a cooled camera for the FOULC application doesn't seem feasible: weight, electric consumption and price.

Another issue that rises in the quantification of some lateral connections is the fact that for the same ratio of T_{LC}/T_F it would be expected to have quantifiable connections for lower values of the ratio Q_{LCIR}/Q_{LC} and non quantifiable for higher values. However, this is not the case for several connections, indicating that there is a certain parameter that affects the consistency of the results, although there is statistical consistency regarding the variance test (Eq. 13). By conducting a sensitivity analysis in order to determine how the changes in the values of independent variables (T_U, T_D, T_{LC}, and Q_U) will affect the uncertainty $\sigma(Q_{LC})$ (dependent variable), it arose that high values of Q_U generate high values of uncertainty, resulting in accepting as quantifiable some experiments with large discrepancies between the estimated and the real discharge of the lateral connections. Figure 19 shows how the uncertainty grows as the flow in the flume increases. The specific experiment is regarded as quantifiable by the proposed method, although the difference between real and estimated discharge of the lateral connection (WL 600mm) is 10.79 l/s.

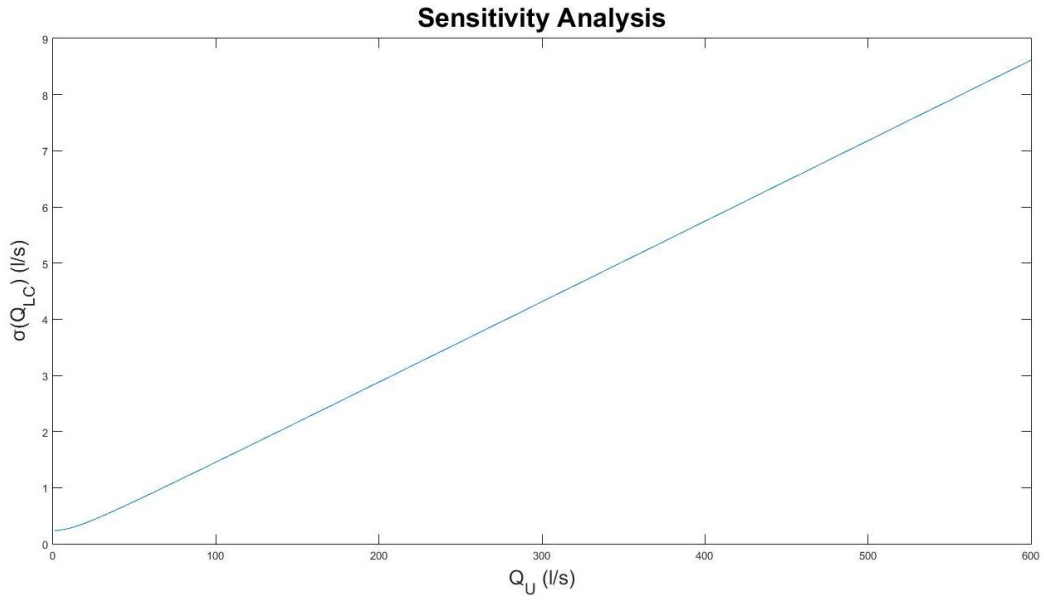

Figure 19. Example of how the uncertainty $\sigma(Q_{LC})$ evolves with respect to Q_U. Discharge in the flume 400 l/s (15.8°C) and a lateral discharge of 0.68l/s (29.3°C) coming through the connection WL 600mm.

Figure 20 depicts the histograms of the difference between the estimated discharges and the real ones of all the quantifiable lateral connections for the different hydraulic conditions. The desired outcome is this difference to be as close to zero as possible for all the experiments, something which occurs only for Q_U=100 & 120 l/s. As the flow in the flume increases, the difference has a tendency to move more away from zero.

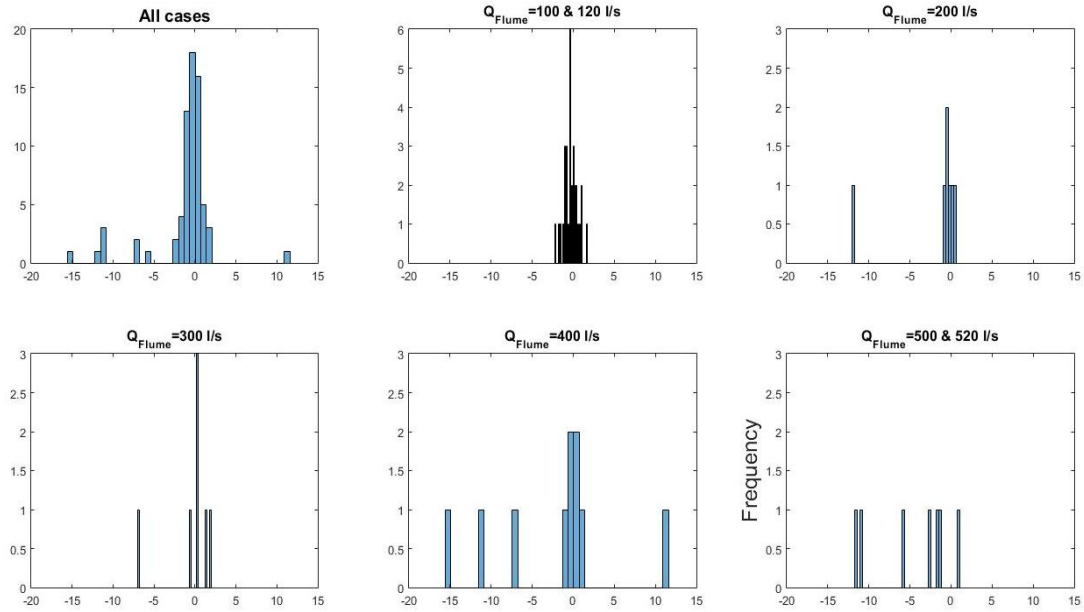

Figure 20. Histograms of the difference between the estimated and the real discharges of all the quantifiable lateral connections ($Q_{LCIR} - Q_{LCReal}$) in l/s, for the tested flows in the flume.

In most of the sewer systems however, the discharges are lower than 100 l/s, a fact that enhances the applicability of the proposed method. Nevertheless, a number of extra experiments with lower discharges could lead to safer conclusions regarding this issue.

4.3. Effect of the moving speed

In order to test whether the moving speed of the train sensor has an impact on the produced results, a triplicate of similar experiments took place. All the conditions were the same, besides some small inevitable differences in the flows of the lateral connections, and the moving speed, which varied from low (~0.3 m/s) to fast (~1 m/s). As it is presented in Figure 21, the detection is possible independently of the moving speed, although the recorded cloud has a different shape. Regarding the quantification of the lateral connection, this special experiment took place only once at a high flow in the flume (400 l/s), a parameter which leads to arbitrary results as it is discussed in session 4.2.

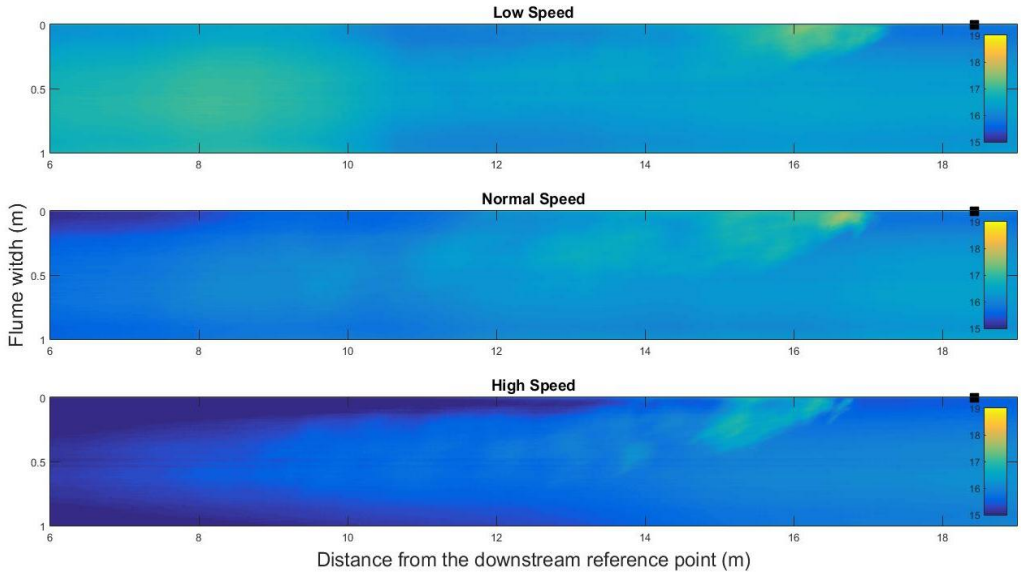

Figure 21. Maps of similar experiments for different moving speeds of the sensor train. Discharge in the flume 400 l/s (15.8°C). Tested connection: WL 600mm. Top map: lateral discharge of 0.68l/s (29.3°C). Middle map: lateral discharge of 0.52l/s (29.3°C). Bottom map: lateral discharge of 0.58l/s (29.3°C).

5. Conclusions and perspectives

An observed crucial fact is that detection of leakage is possible despite the relatively low values of the ratio between the discharge of the lateral connection and the discharge of the flume (Q_{LC}/Q_U), indicating that the detection limits of the technique are expected to be also low. Additionally, it seems to be more feasible to detect illicit connections than groundwater infiltration, mainly due to two reasons: *i)* the way that the foreign fluid is inserted in the pipe (standard connection or diffuser) and *ii)* the density between fluids of different temperatures. A lateral connection (intrusive or normal) is structured in a way that allows more fluid to come out at the same time interval. The groundwater is represented by cold water below 13°C, the illicit connections by warm water above 24°C and the flume's water is in most experiments at circa 15.8°C. Hence, it is expected that, since the infrared camera detects only the temperature distribution on the surface, the presence of colder water can be underestimated or not tracked at all. It is also stressed that connections with higher diameters allow a clearer detection of the source as the fluid is inserted at lower velocities causing a milder mixing with the water in the flume.

The quantification of lateral connections with the proposed method seems to work only for low discharges of the system, mainly due to the dependence of the estimated uncertainties of the lateral connection discharge $\sigma(Q_{LC})$ on the flume's discharge (Q_U). The subjectivity that is inserted in the selection of the point that represents the downstream temperature (T_D) plays also an important role for the correct application of the method. It is also clear that quantification is dependent on the proper operation of the IR camera, as the use of an uncooled camera introduces measurement inconsistencies.

Finally, regarding the FOULC project, it is stressed that the specific IR camera could be an essential part of the hovercraft drone in order to detect active leaking lateral

connections (with the discussed limitations), but quantification seems to be in general hard to achieve (at least for high flows).

6. Acknowledgements

The author would like to thank the assessment committee for the support during the development of this M.Sc Thesis, and Richard Boele and all tab-technicians with Deltares for their support during the experiments.

7. References

de Bénédittis, J. & Bertrand-Krajewski, J.-L., 2005. Infiltration on sewer systems: comparison of measurement methods. *Water Sciences and Technology, 52(3)*, 219 - 227.

Bertrand-Krajewski, J., 2008. Programme rw123etalo: 1st, 2nd and 3rd order polynomial Williamson regression with uncertainties in both variables for sensor calibration, INSA Lyon, LGCIE, Villeurbanne (France).

Bouguet, J.Y., 2004. Camera calibration toolbox for matlab.

Butler, D. and Davies, J., 2004. *Urban drainage*. CRC Press.

Deffontis, S., Breton, A., Vialle, C., Montréjaud-Vignoles, M., Vignoles, C., & Sablayrolles, C., 2013. Impact of dry weather discharges on annual pollution from a separate storm sewer in Toulouse, France. *Sciences of the Total Environment, (452-453)*, 394 - 403.

Chandler, D.M. and Lerner, D.N., 2015. A low cost method to detect polluted surface water outfalls and misconnected drainage. *Water and Environment Journal*, *29*(2), pp.202-206.

Clemens, F. H. L. R., Stanic, N., Van der Schoot, W., Langeveld, J., Lepot, M., 2014. Uncertainties associated with laser profiling of concrete sewer pipes for the quantification of the interior geometry. *Structure and Infrastructure Engineering: Maintenance, Management, Life-Cycle Design and Performance*, DOI: 10.1080/ 15732479.2014.945466

Dirksen, J., Clemens, F. H. L. R., Korving, H., Cherqui, F., Le Gauffre, P., Ertl, T., Plihal, H., Muller, K., Snaterse, C. T. M., 2011. The consistency of visual sewer inspection data. Structure and Infrastructure Engineering, 1-15 iFirst.

Hoes, O.A.C., Schilperoort, R.P.S., Luxemburg, W.M.J., Clemens, F.H.L.R., & van de Giessen, N.C., 2009.Locating illicit connections in storm water sewers using fiber-optic distributed temperature sensing. *Water Research, 43(20)*, 5187 - 5197.

Lega, M., & Napoli, R.M.A., 2010. Aerial infrared thermography in the surface waters contamination monitoring. *Desalination Water Treatment, 23 (1-3)*, 141 - 151.

Lepot, M., Pouzol, T., Aldea Borruel, X., Suner, D. and Bertrand-Krajewski, J.L., 2016. Measurement of sewer sediments with acoustic technology: from laboratory to field experiments. *Urban Water Journal*, pp.1-9.

Nienhuis, J., de Haan, C., Langeveld, J., Klootwijk., M., Clemens, F., 2013. Assessment of detection limits of fiber-optic distributed temperature sensing for

detection of illicit connections. *Water Sciences and Technology, 67(12):2712-8.*

Panasiuk, O., Hedström, A., Marsalek, J., Ashley, R.M., & Viklander, M., 2015. Contamination of stormwater by wasterwater: A review of detection method. *Journal of Environment Management, 152,* 241 - 250.

Reed, B.C., 1989. Linear least-squares fits with errors in both coordinates. *American Journal of Physics*, 57(7), 642-646.

Reed, B.C., 1992. Linear least-squares fitting with errors in both coordinates. II: Comments on parameter variances. *American Journal of Physics,* 60(1), 59-62.

Schilperoort, R.P.S., Gruber, G., Flamink, C.M.L., Clemens, F.H.L.R., & van der Graaf, J.H.M.H., 2006. Temperature and conductivity as control parameters for pollution-based real-time control. *Water Sciences and Technology, 54(11-12),* 257 - 263.

Schilperoort, R., Hoppe, H., de Haan, C., Langeveld, J., 2013. Searching for storm water inflows in foul sewers using fibre-optic distributed temperature sensing. *Water Sciences and Technology,* 68(8):1723-30.

Stanic, N., 2016. *Assessment Methods for Structural and Hydraulic Properties of Concrete Sewer Pipes*. TU Delft, Delft University of Technology.

Williamson, J.H., 1968. Least-squares fitting of a straight line. *Canadian Journal of Physics,* 46, 1845-1847.

8. Appendix A

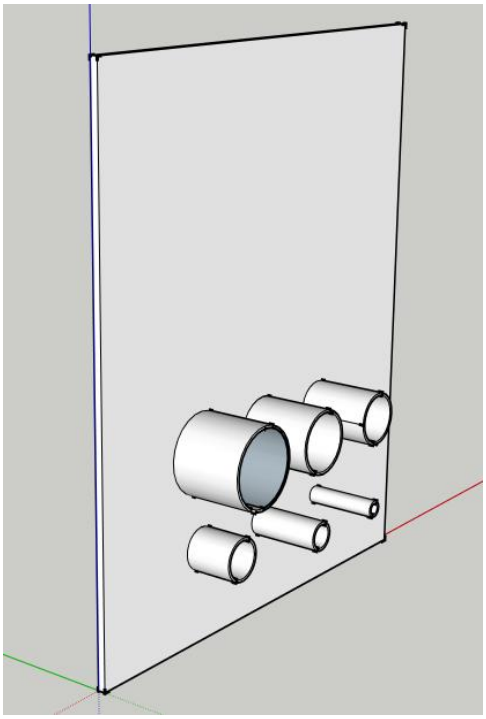

Figure 22. Sketchup© screenshot of the Diameters window.

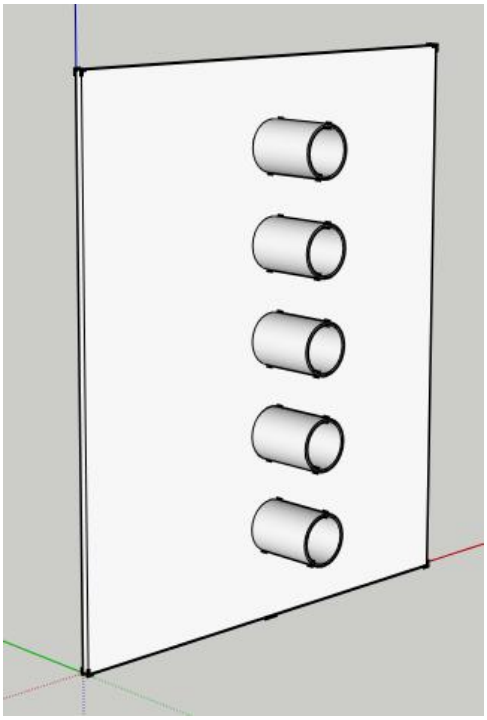

Figure 23. Sketchup© screenshot of the Water Levels window.

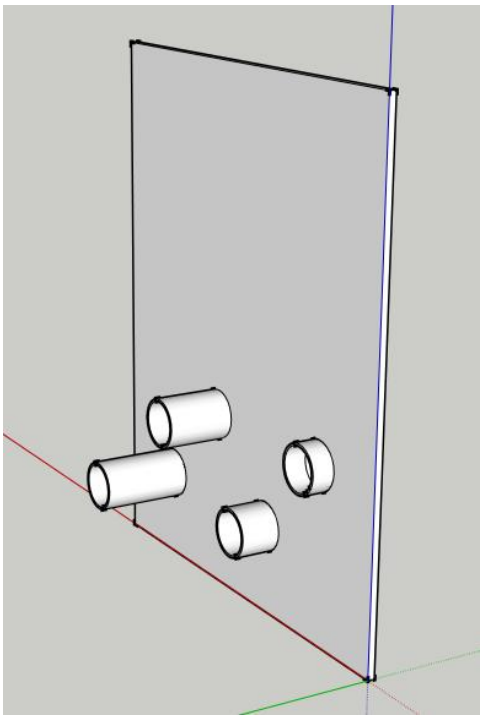

Figure 24. Sketchup© screenshot of the Intrusions window (Side in the flume).

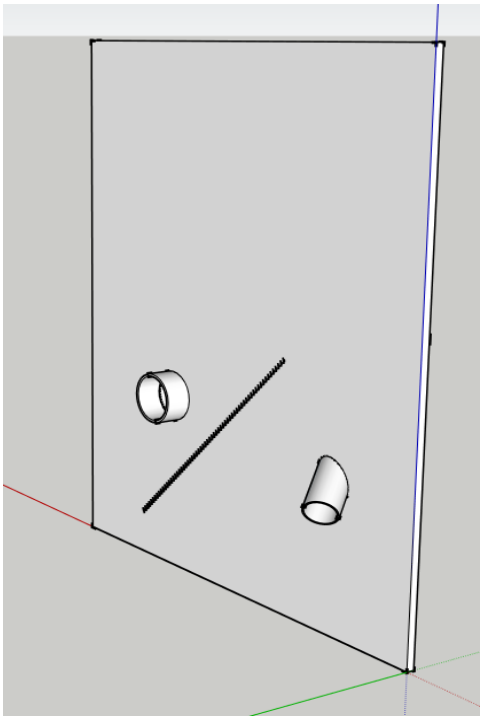

Figure 25. Sketchup© screenshot of the Diameters window (Side in the flume).

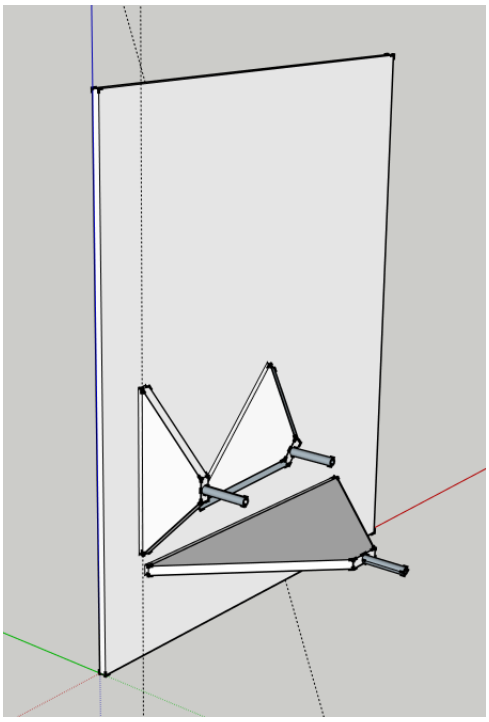

Figure 26. Sketchup© screenshot of the Diffusers window.